HHS Public Access

Author manuscript

Cell Rep. Author manuscript; available in PMC 2023 October 23.

Published in final edited form as:

Cell Rep. 2023 February 28; 42(2): 112043. doi:10.1016/j.celrep.2023.112043.

Elevated PAF1-RAD52 axis confers chemoresistance to human cancers

Sanchita Rauth[1], **Koelina Ganguly**[1], **Pranita Atri**[1], **Seema Parte**[1], **Rama Krishna Nimmakayala**[1], **Venkatesh Varadharaj**[1], **Palanisamy Nallasamy**[1], **Raghupathy Vengoji**[1], **Ayoola O. Ogunleye**[1], **Imayavaramban Lakshmanan**[1], **Ramakanth Chirravuri**[1], **Mika Bessho**[5], **Jesse L. Cox**[2], **Jason M. Foster**[3], **Geoffrey A. Talmon**[2], **Tadayoshi Bessho**[5], **Apar Kishor Ganti**[1,4,5], **Surinder K. Batra**[1,5,*], **Moorthy P. Ponnusamy**[1,5,6,*]

[1]Department of Biochemistry and Molecular Biology, University of Nebraska Medical Center at Omaha, Omaha, NE, USA

[2]Department of Pathology and Microbiology, University of Nebraska Medical Center at Omaha, Omaha, NE, USA

[3]Department of Surgery, University of Nebraska Medical Center at Omaha, Omaha, NE, USA

[4]Division of Oncology-Hematology, Department of Internal Medicine, VA Nebraska Western Iowa Health Care System, University of Nebraska Medical Center, Omaha, NE, USA

[5]Fred and Pamela Buffett Cancer Center, Eppley Institute for Research in Cancer and Allied Diseases, University of Nebraska Medical Center at Omaha, Omaha, NE, USA

[6]Lead contact

SUMMARY

Cisplatin- and gemcitabine-based chemotherapeutics represent a mainstay of cancer therapy for most solid tumors; however, resistance limits their curative potential. Here, we identify RNA polymerase II-associated factor 1 (PAF1) as a common driver of cisplatin and gemcitabine resistance in human cancers (ovarian, lung, and pancreas). Mechanistically, cisplatin- and gemcitabine-resistant cells show enhanced DNA repair, which is inhibited by PAF1 silencing. We demonstrate an increased interaction of PAF1 with RAD52 in resistant cells. Targeting the PAF1 and RAD52 axis combined with cisplatin or gemcitabine strongly diminishes the survival

*Correspondence: sbatra@unmc.edu (S.K.B.), mpalanim@unmc.edu (M.P.P.).

AUTHOR CONTRIBUTIONS

S.R. contributed to designing the project and performed most of the work. K.G. contributed to Figures 2 and 5, through ChIP assay and tumor implantation. P.A. and R.C. contributed to statistical and bioinformatics analysis. S.P., R.K.N., V.V., P.N., A.O.O., and I.L. assisted with some of the work. R.V. contributed to Figure 4 through comet assay and data analysis. M.B. and T.B. have supervised the analysis related to DNA-repair assays. J.L.C. and G.A.T. have performed the pathological analysis and scoring. J.M.F. has provided the fresh tissue samples for organoid generation. A.K.G. has helped with the lung-cancer-related studies. S.K.B. and M.P.P. have supervised and reviewed the manuscript.

SUPPLEMENTAL INFORMATION

Supplemental information can be found online at https://doi.org/10.1016/j.celrep.2023.112043.

DECLARATION OF INTERESTS

S.K.B. is one of the co-founders of Sanguine Diagnostics and Therapeutics, Inc. The other authors declare no competing interests.

potential of resistant cells. Overall, this study shows clinical evidence that the expression of PAF1 contributes to chemotherapy resistance and worse clinical outcome for lethal cancers.

Graphical abstract

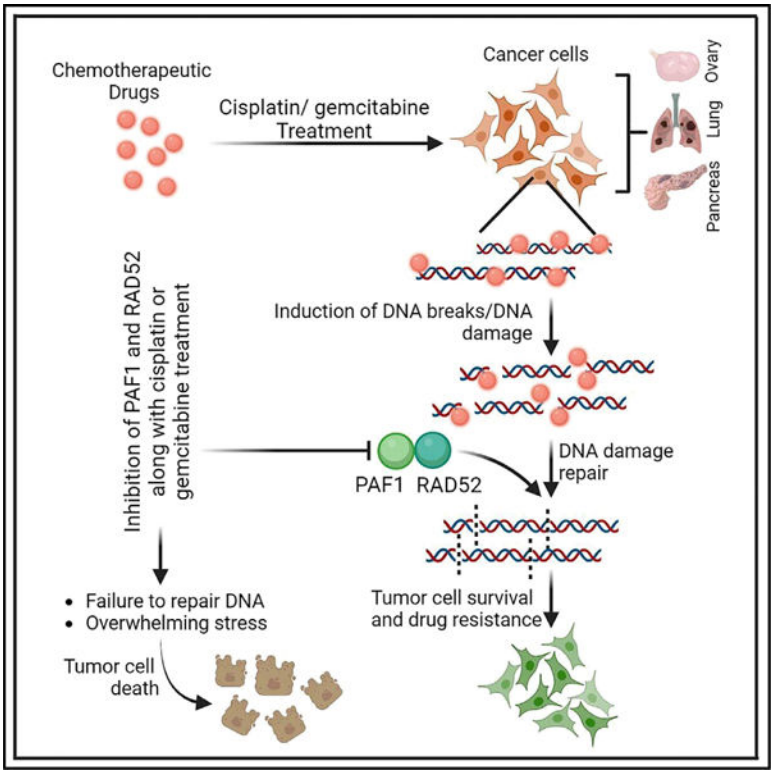

In brief

Resistance to chemotherapies is one of the major challenges in the treatment of aggressive cancers. Rauth et al. report that expression of PAF1 is associated with chemoresistance in ovarian, lung, and pancreatic cancers and interacts with RAD52. Simultaneous targeting of PAF1 and RAD52 sensitizes the cancer cells to chemotherapy.

INTRODUCTION

Chemotherapy prior to or following surgery remains the most used systemic treatment for most cancers. However, the development of chemoresistance in cancer patients confines the successful use of chemotherapeutic drugs. Drug resistance can be developed in many ways; it can be ascended intrinsically from host factors or acquired through genetic and epigenetic variations in the tumor cells.[1–3] Epigenetic alterations can be observed as changes in DNA methylation, acetylation, or histone posttranslational modifications (such as phosphorylation, ubiquitinylation, and SUMOylation) that profoundly affect the expression of genes, resulting in activation or suppression of genes. The rapid development of genetic and epigenetic alterations leads to clonal heterogeneity and facilitates the cancer cells with survival benefits in the presence of chemotherapeutic treatment.[2,4] Moreover,

these alterations can regulate the molecular mechanisms involving increased DNA-repair processes,[5] prosurvival signaling axis,[6] drug metabolisms,[7,8] and increased drug efflux[7] in tumor cells.

Cisplatin-based chemotherapy and others like gemcitabine and 5-fluorouracil have been widely employed to treat various solid tumors, including lung, ovarian, and pancreatic cancers.[9–11] Cisplatin exerts anti-cancer effects through its interaction with DNA and by forming platinum-based DNA adducts, followed by activating the pro-apoptotic signaling pathway.[12] On the other hand, gemcitabine is a deoxycytidine analog that inhibits the DNA polymerase by incorporating it into DNA during replication, which leads to DNA damage and apoptosis.[10] Although still being utilized to treat locally advanced or metastatic cancers, the effectiveness of these drugs is constrained by the development of drug resistance.[13–15] Although a fraction of signaling molecules have been identified as predictive markers of cisplatin or gemcitabine resistance, such as ERBB2, ERCC1, ABCG2, and MYC, most of these studies lacked a clinical correlation or an elucidation for how these proteins provide survival benefits to the cancer cells in the presence of chemotherapeutic drugs.[16–20] Therefore, the identification of a unique protein and dissection of the exact molecular mechanism of chemoresistance are much needed.

RNA polymerase II (RNA Pol II)-associated factor 1/Pancreatic differentiation factor 2 (PAF1/PD2) is a fundamental subunit of the human PAF1 complex (PAF1C), which functions in transcriptional elongation and mRNA maturation by direct interaction with RNA Pol II.[21,22] In addition to its role in transcription, PAF1/PD2 has exhibited its function in tumor progression and cancer stem cell maintenance in different types of cancer, including pancreatic and ovarian cancers.[22–24] Previous studies from our laboratory have illustrated the function of PAF1/PD2 in acinar-to-ductal metaplasia (ADM), an early event contributing to pancreatic cancer initiation.[25] Further, a lung cancer study has shown that aberrant increased expression of PAF1/PD2 can be used as a prognostic marker for early-stage NSCLC, which was found to play a critical role in c-MYC transcriptional activation.[26] Apart from its role in pancreatic, ovarian, and lung cancer pathogenesis, PAF1/PD2 has also been studied in mixed-lineage leukemia (MLL) and cervical cancer.[27,28] Higher PAF1/PD2 expression in pancreatic cancer was correlated with gemcitabine-based drug resistance; however, the detailed molecular mechanisms are still unclear.[29] Further, the function of PAF1/PD2 in cisplatin-based drug resistance has never been explored. Therefore, this study aims to identify the mechanism and characterize the critical function of PAF1/PD2 in cisplatin and gemcitabine resistance in human cancers (ovarian, lung, and pancreatic cancers) and assess its potential as a chemo-sensitizing therapeutic target for the treatment of patients with drug-resistant cancer.

RESULTS

PAF1/PD2 expression correlates with chemotherapy resistance in ovarian, lung, and pancreatic tumors

To examine the potential relationship between PAF1/PD2 expression and chemoresistance in ovarian, lung, and pancreatic cancers, we first quantified the expression of PAF1/PD2 in tumor and normal patient tissue samples. The expression of PAF1/PD2 is significantly

upregulated in all three tumor samples compared with their respective normal tissues as examined by immunohistochemical staining (Figures 1A and 1B). We utilized The Cancer Genome Atlas (TCGA) datasets for ovarian, lung, and pancreatic cancers to examine whether the expression of PAF1/PD2 can be correlated to patient survival. Across the three TCGA cancer types (ovarian, lung, and pancreatic cancers), we found that a small fraction of samples has very high expression of PAF1/PD2 (~2-fold) compared with the median expression of the entire cohort. We further observed that the top 10% of the samples have higher standard deviations than the rest of the cohort. Therefore, we attempted to see if these samples with unusually high expression of PAF1/PD2 bear any prognostic relevance. Our analysis showed that higher expression of PAF1/PD2 is associated with decreased survival of the patients (Figure 1C). PAF1/PD2 expression was further compared between chemotherapy-treated and treatment-naive patient tissue samples to comprehend better the clinical association of PAF1/PD2 with chemoresistance (Table S1). The expression of PAF1/PD2 was upregulated in the chemotherapy-treated group compared with treatment-naive ovarian, lung, and pancreatic cancer patient samples (Figures 1D and 1E). This suggests that the increased PAF1/PD2 may potentially correlate to chemoresistance in cancer cells. To investigate whether PAF1/PD2 is associated with chemotherapy resistance, we generated ovarian (A2780 and 2008), lung (A549 and H292), and pancreatic ductal adenocarcinoma (PDAC) (MIA PaCa2 and SW1990) cell line models with acquired cisplatin and gemcitabine resistance, respectively. For this, wild-type (WT) ovarian, lung, and pancreatic cancer cells were cultured with increasing concentrations of cisplatin (ovarian and lung) and gemcitabine (PDAC) for 6 months (Figure S1A). In concordance with previous observations,[30,31] resistant cells (except H292 and SW1990, which showed more cobblestone-like phenotype) showed highly variable phenotypes from mesenchymal to mixed and epithelial cell types (Figures 1F and S1B). In contrast, WT cells showed more epithelial phenotypes (Figures 1F and S1B). The resistance status of the acquired chemoresistance cells (annotated as CisR and GemR, respectively) was determined by calculating the inhibitory percentage of the cells after treatment with increased concentrations of cisplatin (for ovarian and lung cancer cells) and gemcitabine (for PDAC cells) (Figures 1G and S1C). We observed a reduction in cell death and increased cell proliferation and clonogenic ability of the CisR and GemR cells under cisplatin or gemcitabine treatment (Figures S1D–S1G). qRT-PCR and immunoblotting analysis demonstrated an augmented PAF1/PD2 in chemoresistant cells compared with WT controls (Figures 1H, 1I, and S2A). Together these findings suggest that increased expression of PAF1/PD2 might confer cisplatin and gemcitabine resistance to cancer cells.

Silencing of PAF1/PD2 expression improves cisplatin and gemcitabine sensitivity

We silenced the PAF1/PD2 expression in chemoresistant cells to determine whether PAF1/PD2 has a role in the chemoresistant activity of the cancer cells (Figures 2A and S2B; Table S4). PAF1/PD2 knockdown resulted in the decrease of MDR1 (a drug-resistant marker protein) expression in CisR or GemR cells (Figures 2A and S2B); it might be because PAF1C is a key regulator of MLL1 methyltransferase function, which is further shown to regulate MDR1 gene expression.[32,33] Moreover, depletion of PAF1/PD2 along with cisplatin or gemcitabine treatment significantly reduced the proliferation and increased apoptosis in chemoresistant cells compared with chemotherapy treatment alone (Figures 2B, 2C, S2C,

and S2D). Three-dimensional (3D) tumor organoid models have been widely utilized to study tumor biology and targeted therapies for cancer.[34] Therefore, the effect of PAF1/PD2 inhibition in the 3D tumor organoids of ovarian, lung, and pancreatic cancers was analyzed. Tumor organoid size was significantly reduced under PAF1/PD2 knockdown, along with cisplatin or gemcitabine treatment (Figures 2D and S2E). Moreover, western blotting data showed that the knockdown of PAF1/PD2 with chemotherapy treatment increased the expression of apoptotic markers (Figure 2E).

CisR or GemR cells with corresponding PAF1/PD2 knockdown cells were subcutaneously implanted in both flanks of athymic nude mice to examine whether PAF1/PD2 knockdown affects cisplatin-resistant ovarian and lung tumors and gemcitabine-resistant pancreatic tumors (Figure S2F). Starting at day 7 post-implantation, the ovarian and lung tumor mice were treated with cisplatin or saline, and the pancreatic tumor mice were treated with gemcitabine or saline. We observed no significant reduction in tumor volume in the CisR or GemR tumor-bearing group relative to the control group as a result of cisplatin or gemcitabine treatment, respectively (Figures 2F and 2G). However, chemotherapeutic treatment (cisplatin or gemcitabine) and PAF1/PD2 knockdown reduced the tumor volume in all three cancers (Figures 2F and 2G). No significant changes were observed in the body weight of the mouse when compared between the different treatment groups (Figure S2G). Immunohistochemical analysis with Ki67 and cleaved caspase-3 (CC3) antibodies on the xenograft tumors demonstrate a significant reduction in cell proliferation and increased apoptosis in the combination treatment group compared with the chemotherapy-treatment-alone group, thereby corroborating the observations from our *in vitro* experiments (Figures 2H and 2I).

In addition to chemoresistant cells, we analyzed the effect of PAF1/PD2 knockdown (Figure S3A) along with chemotherapy treatment in the parental cells. Treatment with cisplatin or gemcitabine alone decreases the proliferation and apoptosis of the parental cells (Figures S3B and S3C). Moreover, we observed no noticeable changes in proliferation or apoptosis between the combination (PAF1/PD2 knockdown along with cisplatin or gemcitabine) group and only the chemotherapy-treated group (Figures S3B and S3C). To examine whether overexpression of PAF1/PD2 could mitigate the chemotherapy efficacy and increase chemoresistance in the parental cells, we transfected A2780, A549, and MIA PaCa2 WT cells with PAF1/PD2-expressing plasmid (Figure S3D). Overexpression of PAF1/PD2 increased the resistance of A2780 and A549 cells to cisplatin and MIA PaCa2 cells to gemcitabine (Figures S3E and S3F).

RAD52 is a partner protein of PAF1/PD2

To elucidate the underlying mechanism of PAF1/PD2 in the regulation of chemoresistance, we performed mass spectrometry analysis on the resistant cells to identify proteins associated with PAF1/PD2 (Figure 3A). Followed by mass spectrometry, the interactome protein profiles between the A2780 CisR, A549 CisR, and MIA PaCa2 GemR cells were compared. We identified ~33 common proteins that interact with PAF1/PD2 in all three chemoresistant cells (Figure 3B; Table S5). Pathway enrichment analysis using the interactome proteins (~33 common proteins) from the mass spectrometry dataset

showed that the proteins were enriched in pathways such as the DNA-damage response (DDR) pathway, pyrimidine synthesis, and homologous recombination (HR) (Figure 3C; Table S5). Among the common interacting proteins between all three cell lines, RAD52, a DNA-repair protein, was identified to be binding with PAF1/PD2 in the resistant cells (Figure 3D). Previous studies have illustrated the involvement of mammalian RAD52 in homology-directed (HR) and single-stranded annealing (SSA) double-strand break (DSB) repairs, RNA-DNA hybrid structures, and transcription-mediated DNA-repair processes.[35–38] RAD52 has also been implicated in counteracting excessive fork regression by activating break-induced replication (BIR) and cooperates with various nucleases, such as MRE11 and MUS81, to promote DNA replication under replication stress.[38–40] These compensatory roles in the resolution of DSBs and at replication forks of RAD52 are utilized by cancer cells as a survival strategy under drug treatment conditions.[41–43] We investigated this interaction because mass spectrometry suggested a close association of PAF1/PD2 with RAD52.

Immunoprecipitation assay confirmed the interaction of PAF1/PD2 with RAD52 in chemoresistant and control cells (Figures 3E and S4A). Furthermore, the expression of RAD52 is also increased concomitant with PAF1/PD2 in CisR and GemR cells. Consecutively, analysis using proximity ligation assay (PLA) on HeLa cells showed an increased association of PAF1/PD2 and RAD52 on cisplatin treatment (Figures 3F and 3G). Next, immunohistochemical staining (on the same tissue array, i.e., used in Figure 1A) revealed an increased expression of RAD52 in the tumor sample compared with normal tissue samples (Figure 3H). Furthermore, co-localization of PAF1/PD2 and RAD52 was also evident in the ovarian, lung, and pancreatic cells and tumor samples (Figures S4B and S4C). To determine whether RAD52 expression is correlated with chemoresistance, we performed immunohistochemical analysis on the chemotherapy-treated and treatment-naive patient tissue samples. Although we observed a higher expression of RAD52 in the chemotherapy-treated patient samples than in the non-chemotherapy-treated tissues, the result was insignificant (Figure S4D). Collectively, these data demonstrated that PAF1/PD2 interacts with RAD52 and might play a role in chemoresistance.

PAF1/PD2 promotes DNA repair after chemotherapeutic treatment

Chemotherapeutic agents directly or indirectly induce DNA damage to induce tumor cell death;[44,45] thus, DNA-damage-repairing potential profoundly affects the sensitivity of tumor cells to chemotherapies. Further, our data represent the interaction of PAF1/PD2 with RAD52; therefore, PAF1/PD2 may function in the DNA-repair and/or DDR pathway. HeLa and U2OS cell lines have been widely used as cellular models for the studies of DNA-damage and DNA-repair pathways;[46] thus, in few experiments, we have used these two-cell lines to examine the role of PAF1/PD2 and RAD2 in DNA damage. Hydroxyurea (HU) is widely used as a reagent to study DNA damage;[47,48] therefore, to investigate whether PAF1/PD2 has any function in the DDR pathway, HeLa cells were treated with HU (4 mM) for 4 h to induce DSBs. In response to HU, an increased nuclear expression of PAF1/PD2 was observed using an immunofluorescence assay (Figures S5A and S5B). Considering that chemoresistant cells have elevated DNA-repair activity compared with control cells to resist cell death during chemotherapy treatment, we evaluated the overall DSBs via neutral

comet assay. Under treatment with cisplatin or gemcitabine, the chemoresistant A2780 CisR, A549 CisR, and MIA PaCa2 GemR cells showed lower levels of DNA damage than WT cells (Figures S5C and S5D). Next, to determine whether PAF1/PD2 affects DNA repair, we exposed the PAF1/PD2 knockdown cells to cisplatin or gemcitabine, respectively, and performed a neutral comet assay after 48 h of treatment. PAF1/PD2 knockdown cells showed higher levels of DSBs, as demonstrated by the appearance of longer tails than chemoresistant control cells (Figures 4A and 4B). We also observed that overexpression of PAF1/PD2 in the parental cells reduced the DBSs in the cells (Figures 4C and 4D). Interestingly, the treatment with cisplatin (A2780 and A549 cells) and gemcitabine (MIA PaCa2 cells) increased the recruitment of PAF1/PD2 and RAD52 to chromatin in the chemoresistant cells (Figure 4E). Consistent with these observations, the treatment with cisplatin or gemcitabine on the PAF1/PD2 knockdown chemoresistant cells resulted in the accumulation of DNA damage, as documented by the elevated H2AX phosphorylation (YH2AX) (Figure 4F). We also observed co-localization of PAF1/PD2 with YH2AX in HeLa cells on treatment with cisplatin (Figure 4G). Furthermore, immunohistochemical analysis of the xenograft tumors revealed an upregulation of YH2AX expression in the PAF1/PD2 knockdown tumors treated with cisplatin or gemcitabine, confirming *in vitro* findings (Figures S5E and S5F).

HR and non-homologous end joining (NHEJ) are the main DSB-repair pathways, so we evaluated whether PAF1/PD2 affects these pathways using a cell-based DSB-repair assay. U2OS-driven cell lines that can specifically detect HR (U2OS-DR), NHEJ (U2OS-EJ5), and SSA (U2OS-SA) were used.[49] Depletion of PAF1/PD2 (Figure S5G) resulted in a marginal reduction of the percentage of GFP-positive cells in both HR and NHEJ (Figure 4H). Because one of the major interactome proteins found through mass spectrometry is RAD52, we evaluated the role of PAF1/PD2 in the RAD52-mediated SSA-repair pathway. Silencing of PAF1/PD2 significantly reduced the percentage of GFP-positive cells (Figure 4H), demonstrating that loss of PAF1/PD2 impairs the proficiency of DNA repair in cells. Combining these results suggests that PAF1/PD2 might promote DNA repair to render cancer cells more resistant to chemotherapeutic agents. Considering that HU can affect the cell-cycle profile of the cells, we tested the effect of 4 mM HU in cells after 4 h of treatment. Cell-cycle profiling shows no noticeable changes after 4 h of treatment compared with 0 h (Figure S5H).

PAF1/PD2 partly regulates the RAD52-mediated DNA-damage repair

Based on the above discoveries that PAF1/PD2 interacts with RAD52 and is correlated to DNA repair, we questioned whether PAF1/PD2 is necessary for RAD52-mediated DNA-repair functions. First, we observed that silencing of PAF1/PD2 did not affect RAD52 expression (Figure S6A). The DNA-repair activity of RAD52 is often monitored by the DNA-damage-dependent formation of subnuclear foci.[50] Therefore, we tested whether PAF1/PD2 could affect the DNA-damage-induced RAD52 foci formation. Silencing PAF1/PD2 in HeLa cells with GFP-RAD52 (Figure 5A) dramatically reduced the RAD52 foci formation in response to HU (Figures 5B and 5C). Furthermore, treatment with either cisplatin (in A2780 CisR and A549 CisR) or gemcitabine (MIA PaCa2 GemR) significantly induced the formation of RAD52 foci (Figures S6B and S6C). However, the silencing of

PAF1/PD2 in the resistant cells significantly reduced the number of RAD52 foci (Figures 5D and 5E). We further examined the effects of PAF1/PD2 on foci formation of other DSB-repair factors, RAD51, CtIP, and total and phospho-RPA.[38] Transient knockdown of PAF1/PD2 significantly reduced the number of RAD51 and CtIP foci in response to HU treatment, as shown in Figures 6D–6G; however, neither total nor phospho-RPA32 foci formation showed any changes. Moreover, our western blotting analysis showed that PAF1/PD2 silencing has no effects on the protein expression of CtIP, RAD51, and total or phospho-RPA32 (Figure S6A).

Given the involvement of PAF1/PD2 in the RAD52 DNA-repair activity, we asked whether inhibition of PAF1/PD2 would affect the recruitment of RAD52 to chromatin following genotoxic treatment. Treatment with HU, cisplatin, or gemcitabine increased the PAF1/PD2 and RAD52 binding to chromatin, but inhibiting PAF1/PD2 expression significantly reduced RAD52 accumulation at chromatin in response to treatment (Figures 5F and 5G). The binding of RAD52 to transcriptionally active genes (GAPDH and ACTB) was analyzed with chromatin immunoprecipitation (ChIP) assay in PAF1/PD2 knockdown and control cells to consolidate these findings further. Treatment with cisplatin augmented the binding of PAF1/PD2 and RAD52 on the genes (Figure 5H) compared with non-cisplatin-treated control cells. However, silencing of PAF1/PD2 inhibits the association of RAD52 to genes on treatment with cisplatin (Figure 5I).

Inhibition of PAF1/PD2, along with RAD52, imparts higher drug sensitivity

Because we found that PAF1/PD2 is involved in DNA repair and has an association with RAD52 in chemoresistant cells, we hypothesized that inhibiting RAD52 DNA-repair activity in combination with PAF1/PD2 silencing could promote tumor cell death. To test this possibility, we evaluated the inhibition of RAD52-DNA-repair activity on the chemoresistant cells by treating them with D-I03. D-I03 specifically impedes RAD52-dependent SSA, thus obstructing the DNA-repair activity of RAD52.[51,52] Real-time kinetics assay demonstrates that silencing of PAF1/PD2 and RAD52 together with cisplatin or gemcitabine treatment significantly inhibits the proliferation and increases the apoptosis of the chemoresistance cells (Figures 6A, 6B, and S7A). In addition, we also treated these cells with cisplatin or gemcitabine alone or a combination of D-I03 with cisplatin or gemcitabine, and we observed that cisplatin or gemcitabine alone had little effect on inhibiting the cell proliferation; however, combined treatment of cisplatin or gemcitabine with D-I03 suppressed cancer cell growth (Figures S7B and S7C). Further observation showed a decline in the clonogenic potential of resistant cells when treated with cisplatin or gemcitabine in combination with D-I03 and PAF1/PD2 knockdown (Figure 6C). Our combination index (CI) plot revealed a combination to synergistic effect on cell viability on combining D-I03 with cisplatin or gemcitabine treatment in chemoresistant cells (Figure S7D). Moreover, western blotting showed that treatment of chemotherapeutic drugs and D-I03 with PAF1/PD2 knockdown induced the expression of CC3 and YH2AX (Figure 6D). Comparable effects on the resistant cells were also observed using another RAD52 inhibitor, mitoxantrone (MTX)[52] (Figure S7E). Consistent with our cellular studies, we observed that treatment of tumor organoids with PAF1/PD2 small interfering RNA (siRNA), D-I03, and cisplatin or gemcitabine alone has a minimal effect on the organoid's growth (Figures 6E, 6F, and

S7F). However, combination treatment of PAF1/PD2 knockdown along with D-I03 and chemotherapeutic drugs (cisplatin or gemcitabine) imposed a striking effect on increasing tumoroid death compared with single treatment alone (Figures 6E and 6F). The loss of organoid viability in the combination treatments was further associated with increased accumulation of apoptosis and DNA damage, as examined by CC3 and YH2AX levels (Figure 6G).

PAF1/PD2 predicts chemotherapy vulnerability of ovarian, lung, and pancreatic cancers

We examined PAF1/PD2 expression and its relationship with cisplatin or gemcitabine resistance in multiple ovarian, lung, and pancreatic cancer cell lines. For these, we correlated the levels of PAF1/PD2 protein from the multiple cancer cell lines with the half-maximal inhibitory concentration (IC_{50}) of cisplatin and gemcitabine, respectively. We observed that cisplatin or gemcitabine resistance directly correlates with the expression of PAF1/PD2 (Figures 7A and S8).

To demonstrate whether our findings have clinical relevance, we evaluated PAF1/PD2 levels in paired pre- and post-chemotherapy-treated ovarian, lung, and pancreatic cancer patient samples. Further, the expression of PAF1/PD2 in the tumors was compared with the clinical responses to chemotherapy (Table S3). PAF1/PD2 levels were significantly higher in the post-chemotherapy treatment group for ovarian cancer and pancreatic cancer than in the pre-chemotherapy treatment group (Figures 7B and 7C). However, the post-treatment tissue samples showed reduced PAF1/PD2 levels in the lung cancer patient cohort (Figures 7B and 7C), probably as a result of the small sample size. Although PAF1/PD2 expression changed in most cases, patients with a poor response to the chemotherapy showed significantly increased expression in the post-chemotherapy tissues compared with respective pre-chemotherapy tissues (Figure 7D). Further analysis of the same cohorts showed that the high expression of PAF1/PD2 after chemotherapy treatment was associated with a worse response to chemotherapy in patients, and reduced PAF1/PD2 expression post-chemotherapy is correlated with a better response to chemotherapy (Figure 7D). Altogether, we reason that PAF1/PD2 may act on DNA repair and promote chemoresistance in ovarian, lung, and pancreatic cancer patients.

DISCUSSION

Resistance to chemotherapeutic drugs is one of the major challenges to the failure of treatments in cancer patients. Although patients' initial response to chemotherapy is often effective, relapse with drug-resistant cancer usually occurs, and patients surrender to the disease.[53] Cisplatin or gemcitabine, alone or in combination with other drugs, is used as a treatment regimen for many cancers. Multiple molecular mechanisms of chemotherapy resistance encompassing different pathways have been studied; however, identifying a molecular mechanism that can be targeted in a broader aspect has never been addressed. In the current study, we demonstrated PAF1/PD2 as a key factor in regulating cisplatin and gemcitabine resistance in human cancers using ovarian, lung, and pancreatic cancers as study models. Our findings suggest a mechanistic basis by which PAF1/PD2 assists tumor cells to evade chemotherapy-induced cell death and enhance tumor cell proliferation.

Mechanistically, PAF1/PD2 reduces DNA damage, probably by facilitating the activity of RAD52 to enhance the repair of chemotherapy-induced DNA damage. Moreover, we found a diminution in RAD52 foci formation and its binding to chromatin on the knockdown of PAF1/PD2. Inhibition of RAD52 by small-molecule inhibitors D-I03 or MTX, along with PAF1/PD2 silencing, enhances the apoptosis of the tumor cells to cisplatin or gemcitabine. Using clinical samples, we discovered that upregulation of PAF1/PD2 correlates with poor chemotherapy response. Hence the PAF1/PD2-RAD52 axis may serve as a target for improving the efficacy of chemotherapy.

Primary treatments, including chemotherapy or radiation therapy, induce cell death by directly or indirectly causing DNA damage; thus, enhancing the DNA-repair activity may contribute to the resistance of cancer cells to genotoxic agents.[54–56] RAD52, which showed an interaction with PAF1/PD2, was identified using an unbiased proteomic analysis to identify PAF1/PD2-binding proteins in chemoresistant cells. Previous studies have suggested the association of PAF1C with DNA recombination and repair processes.[57–61] Moreover, separate studies on PAF1C and RAD52 have shown the interaction of these two proteins with similar kinds of DNA-repair proteins (such as CSB and MRE11)[37,59] or DNA-repair pathways.[38,59,62] Our data indicate an interaction of PAF1/PD2 to RAD52 in the chemoresistant cells. Furthermore, we have uncovered the role of PAF1/PD2 in the DSB-repair pathway.

Mammalian RAD52 has been involved in the various DNA-repair processes, including SSA and HR repair of DSBs, preventing excessive degradation of the stalled replication fork, and in transcription-associated DNA repair.[38,63,64] Due to its compensatory roles in the resolution of DNA-damage repair, RAD52 has been implicated in developing drug resistance, including resistance to platinum-based chemotherapy.[65,66] In addition, RAD52 has also been shown to be associated with tumor progression and cancer risk.[66–68] In line with the previous studies, we also observed that RAD52 is substantially upregulated in ovarian, lung, and pancreatic tumor samples. Further, significant DNA damage was detected in the PAF1/PD2-depleted cells, and a decrease in overall DNA damage was observed following PAF1/PD2 overexpression. Notably, the depletion of PAF1/PD2 significantly reduces the SSA-repair process; this could be caused by the inhibitory effect of PAF1/PD2 depletion on RAD52-SSA-mediated DNA-repair activity. This is further supported by the fact that RAD52 foci and their recruitment to chromatin are reduced when PAF1/PD2 is depleted in cells treated with HU, cisplatin, or gemcitabine. Based on our results, we suggest that PAF1/PD2 might be important for binding RAD52 to chromatin in response to HU or chemotherapy-induced DNA lesions; however, this notion needs further validation. Despite the fact that we found a greater physical interaction between PAF1/PD2 and RAD52 in chemoresistant cells, it would be intriguing to determine the mechanism of PAF1/PD2 and RAD52 interaction in further research. In addition to RAD52, the suppression of PAF1/PD2 significantly reduces the foci formation of CtIP and RAD51 without altering the foci formation of RPA on HU treatment. RAD51 is an essential recombination in HR.[69] CtIP promotes the resection of the DSB ends by the MRE11 to generate 3′-single-strand tails to initiate HR.[70] The CtIP/MRE11-mediated resection is also essential for SSA and micro-homology-mediated end joining (MMEJ).[71] These data suggest that PAF1/PD2 is also involved in DSB repair in a RAD52-independent manner because CtIP and RAD51 do not

require RAD52 for their activities. Another interesting result we observed using pathway enrichment analysis is that proteins involved in purine metabolism that have roles in DNA-damage-repair pathways and therapy resistance interact with PAF1/PD2 in chemoresistant cells.[72,73] These findings not only add to our understanding of the function of PAF1/PD2 in DNA repair, but they also raise the possibility that PAF1/PD2 overexpression may be necessary to repair chemotherapy-induced DNA damage in chemoresistant cancer cells, giving them a survival advantage under continued drug pressure. Given that the PAF1/PD2 inhibitor is currently unavailable, the RAD52 DNA-repair pathway is druggable and may serve as an alternative target for reversing the chemotherapeutic resistance of tumor cells. Indeed, we found that combining a RAD52 inhibitor with cisplatin or gemcitabine increased the sensitivity of chemoresistant tumor cells and tumor organoids to chemotherapeutic drugs. Considering these findings, we expect that RAD52 inhibitors could act as a potent sensitizer for targeting chemoresistant cancers with PAF1/PD2 overexpression. Moreover, studies have demonstrated that simultaneous targeting of RAD52 and PARP exerted a synergistic effect against a variety of solid tumor cells.[52,74] Because Poly (ADP-ribose) polymerases (PARP) inhibitors, like olaparib or niraparib, are widely used to treat several cancers,[75] it would therefore be interesting in the future to study the synergistic effect of PARP and RAD52 inhibitors in chemotherapy-resistant tumors.

In addition to the biological significance of PAF1/PD2, our work may be relevant in the clinical management of chemotherapy-resistant patients. Because the magnitude of PAF1/PD2 expression is correlated with the risk of tumor and poor response to chemotherapy, the measurement of PAF1/PD2 post-chemotherapy may be an effective approach to predict patient response to treatment and thus serve as an excellent reference marker. Thus, targeting PAF1/PD2 could overcome cisplatin or gemcitabine resistance.

Limitations of the study

We identified that PAF1/PD2 interacts with and regulates the DNA-repair activity of RAD52 in chemoresistance cells, but it is still unknown which domains of these molecules contribute to the interaction. Further, our research on how PAF1/PD2 regulates RAD52 DNA-repair function did not define the detailed molecular mechanism underlying chemoresistance. In addition, we did not address how RAD52 could affect the PAF1/PD2 chemoresistance and DNA-repair function in tumor cells, which would be of great significance in explaining the role of these two molecules in mediating drug resistance on chemotherapy treatment. Lastly, we have a small number of samples to confirm the correlation between PAF1/PD2 expression and chemotherapy response in ovarian, lung, and pancreatic cancer patients.

STAR★METHODS

RESOURCE AVAILABILITY

Lead contact—Further information and request for resources should be directed to and will be fulfilled by the Lead contact, Moorthy P. Ponnusamy (mpalanim@unmc.edu).

Materials availability—Materials, including cell lines (except the U2OS-DR, U2OS-EJ5, and U2OS-SA), are available from the lead contact with a completed Material Transfer Agreement.

Data and code availability—Mass spectrometry data have been deposited to Pride ProteomeXchange with Project accession: PXD039281, and Project https://doi.org/10.6019/PXD039281.

This paper does not report original code.

Any additional information related to this manuscript is available from the lead contact upon request.

EXPERIMENTAL MODELS AND SUBJECT DETAILS

Patients and clinical Specimens—All the human samples were obtained post-approval of the protocol by the Institutional Review Board (IRB) at the University of Nebraska Medical Center, Omaha, Nebraska. All clinical samples were collected with informed consent from the patients before sample collection following institutional guidelines. Paraffin-embedded deidentified human ovarian, lung, and pancreatic cancer tissue samples (from chemotherapy-treated and treatment naive groups) were obtained from the UNMC tissue bank. All the relevant information on the patients with treatment history used for immunohistochemical staining can be found in Tables S2 and S3. For patient samples used in Figure 7, were collected from both male and female between ages 44 to 80 (Table S3). The tissues were collected before therapy (pre-therapy) and after therapy (post-therapy). The chemotherapy response of the patients was determined by the UNMC pathologists based on the post-therapy stage (Table S3). Fresh tissue from pancreatic tumor and ovary metastatic (omentum) samples were used to generate 3D organoids. The clinical tissue slides from ovary, lung and pancreatic tumor samples were used to determine the levels of PAF1/PD2 and RAD52.

Mice—Male and female athymic nude mice aged 6 weeks were used for the study. Animal Animal experiments were performed according to the protocol approved by the Institutional Animal Care and Use Committee of the University of Nebraska Medical Center, Omaha, Nebraska.

Cell lines—All cell lines were authenticated using STR DNA profiles and verified for mycoplasma-free status every month. All pancreatic and ovarian cancer cell lines were cultured in Dulbecco's Modified eagle's medium (DMEM; 4.5 mg/mL glucose) with 10% FBS. All lung cancer cell lines were cultured in RPMI 1640 medium supplemented with 10% FBS and 1% penicillin/streptomycin.

Cells were incubated in a humidified incubator at 37°C and supplied with 5% CO2. During the *in vitro* experiments, the respective concentration of cisplatin, 4μM for A2780 CisR, 2008 CisR, and A549 CisR, 2μM for H292 CisR were used. And for MIAPaCa2 GemR and SW1990 GemR cells were treated at a concentration of 2μM and 1μM of gemcitabine, respectively.

Subcutaneous tumor implantation—Cisplatin- or gemcitabine-resistant cells alone or with PAF1/PD2 knockdown (1X 10^6 cells/flank) were suspended in 500 μL of PBS and mixed with matrigel in 1:1 ratio. Cells in 100 μL volume (Matrigel-PBS mixture) were injected subcutaneously into the right and left flanks of six-week-old athymic nude mice. Three mice were used for each group. Cisplatin (5 mg/kg) and gemcitabine (1.5 mg/kg) twice a week were administered by intraperitoneal (I.P) injection to the indicated group, respectively. Treatment was started at the onset of the tumor, and the tumor volume was measured once every three days. Tumors were resected on Day 24, and tumor weight was measured. Tumor sections were stained with cleaved caspase 3, Ki67, and YH2AX; Ki67 and YH2AX were scored by the pathologist, and for cleaved caspase 3, five images were randomly taken for each slide, followed by manual counting of the number of cleaved caspase 3 positive cells in each field.

METHOD DETAILS

Generation of PAF1/PD2 stable knockdown (shRNA) cell lines, siRNA transfection and PAF1/PD2 overexpression—The sh-RNA mediated stable knockdown of PAF1/PD2 was performed in A2780 CisR, A549 CisR, and MIA PaCa2 GemR cells, and respective controls were transfected with Scr. The shRNA sequence targeting PAF1/PD2 is shown in Table S4. HEK293T cells were transfected with PAF1/PD2 shRNA constructs and Lipofectamine 20,000 to generate the viral particles according to the manufacturer's protocol. Then the supernatant was collected after 48 h and 72 h; the supernatant was used to infect the cells using polybrene. After 48 h of infection, the PAF1/PD2 stable knockdown cells were selected against puromycin (4 μg/mL). For PAF1/PD2 overexpression, A2780, A549, and MIApaCa2 cells were transfected with lentiviral vector carrying PAF1/PD2, and respective controls were transfected with Vector control using the same protocol as mentioned above.

The transient knockdown of PAF1/PD2 was performed with PAF1/PD2 small interfering RNAs (siRNAs), which is a pool of three target-specific (27mer siRNA duplexes) sequences. A concentration of 10 nM for each sequence was used for the transfection. Lipofectamine 2000 was used for every transfection and performed according to the manufacturer's.[22] For the transient knockdown of PAF1/PD2 in organoids, we have followed the protocol mentioned by Dekkers et al.[76] The organoids were dissociated using TryLE and pelleted via centrifugation at 300g for 5 min. The dissociated organoids were resuspended in 450 mL of organoid-specific media and transferred into a 24-well suspension plate. The SCR and siPAF1 RNAs were mixed with Lipofectamine 2000 in two Eppendorf tubes following the manufacturer's protocol and incubated at room temperature for 20 min. After incubation, the transfection mix was added to the dissociated organoid. The transfection mix and the organoids were mixed gently by pipetting up and down and incubated at 37°C in 5% CO_2 for 4 h. After incubation, the organoids were collected in tubes, centrifuged at 300g for 5 min, and plated with matrigel for further growth. The knockdown was analyzed using RT-PCR following 48 h of transfection.

MTT cytotoxicity assay—A total of 3000 cells/well were seeded in 96 well plates 24 h before the treatment. The cells were treated with the indicated concentration of

cisplatin or gemcitabine for 48 h. After 48 h of treatment, 3-[4,5-dimethylthiazol-2-yl]-2,5-diphenyltetrazolium bromide (MTT, 5 mg/ml) agent was added for 4 h. The medium was then removed, and 200 μL/well DMSO was added. Relative toxicity was determined by measuring the absorbance at 570 nm using a plate reader (BMG Labtek).

Combination index (CI)—The combination effects or index (CI) of cisplatin or gemcitabine along with PAF1/PD2 knockdown and D-I03 was calculated using CompuSyn software after performing the MTT assay using cisplatin or gemcitabine and D-103.[77] A CI value < 1 represents a synergistic effect, whereas a CI value = 1 or >1 indicates additive and antagonistic effects.

Histology, Immunohistochemistry, and immunofluorescence—Xenograft tumors from mice were fixed in 10% paraformaldehyde overnight and embedded in paraffin. The maximum cross-sections (4 μm thick) were picked for slide preparation. Immunohistochemical analysis was carried out with the following primary antibodies: rabbit polyclonal anti-PAF1/PD2 (Bethyl Laboratories, IHC-00378, 1:200), rabbit polyclonal anti-RAD52 (Abcam, ab117097, 1:50), rabbit polyclonal Ki67 (cell signaling, 12202S, 1:300), rabbit polyclonal anti-cleaved caspase 3 (cell signaling, 9661L, 1:400), and rabbit monoclonal anti-YH2AX (Cell Signaling, 9718S, 1:400). The tissue sections were rehydrated by immersing the slides in xylene, and 100%, 90%, 70%, 50%, and 30% ethanol (each for 5 min). Finally, the slides were rinsed with deionized water for 5 min and proceeded for antigen retrieval using citrate buffer (pH 6.0). Following antigen retrieval, the slides were washed with deionized water and incubated overnight at 4°C. The next day, the sections were washed with PBST, and HRP-conjugated secondary antibodies were added; the signal was developed using DAB. Following DAB, the slides were counterstained with Mayer's hematoxylin. The pathologists carried out histological analyses, and the demonstrated immunohistochemical image was representative of the indicated group. The staining intensity was assigned as follows: 0, negative; 1, weak; 2, medium, and 3 strong.

Organoids and cells were fixed in methanol for 2 min, then permeabilized for 5 min in 0.025% Triton X-100/PBS for immunofluorescence staining. After blocking in 3%-BSA/PBS, organoids and cells were stained with mouse monoclonal anti-PAF1/PD2 (in-house generated, 1:200) or rabbit polyclonal anti-PAF1/PD2 (Abcam, ab20662, 1:300), mouse monoclonal anti-RAD52 (Santacruz, sc-365341, 1:200), rabbit polyclonal anti-GFP (Novus Biologicals, NB600-308, 1:200), rabbit monoclonal anti-RAD51 (Abcam, ab133534, 1:50), rabbit monoclonal anti-total RPA32 (Abcam, ab109084, 1:100), rabbit polyclonal anti-phospho RPA32 (Bethyl Laboratories, A300-245A, 1:200), mouse monoclonal anti-CtIP (Santacruz, sc-271339, 1:50), rabbit monoclonal anti-YH2AX (Cell Signaling, 9718S, 1:400) and rabbit polyclonal anti-cleaved caspase 3 (Cell Signaling, 9661L, 1:400). Following primary antibody incubation overnight at 4°C, the samples were incubated with anti-mouse or -rabbit Alexa 488/563-conjugated secondary antibody. After mounting with DAPI vectashield, images were acquired using Zeiss LSM800 confocal microscope with 63 ×/1.4 NA or 40 × NA oil objective (Carl Zeiss Microimaging). The foci were counted manually in 30–100 cells for each group, and the immunofluorescence image represented the indicated group. The PAF1/PD2 nuclear intensity was measured using ImageJ software.

Immunoprecipitation and immunoblot assay—Protein lysates were collected using CHAPS protein lysis buffer (50 mM Pipes/HCl, ph6.5; 2 μM EDTA, 0.1% CHAPS, 20 μg/mL Leupeptin, 10 μg/mL Pepstatin A, 10 μg/mL Aprotinin) and processed for immunoprecipitation and immunoblotting.[21] For western blotting, the protein lysates were mixed with 6X protein loading buffer and boiled for 5 min. 30 μg of protein concentration was loaded onto 10% polyacrylamide gel (PAGE). For immunoprecipitation, the antibody was incubated with 20 μL of Dynabeads for 1 h at room temperature, and then 500 μg of protein lysates were incubated with antibody-bounded Dynabeads overnight at 4°C. Next day, the beads were washed three times with CHAPS buffer, and the samples were eluted in 50 μL of 2X-SDS PAGE gel loading buffer by heating the sample at 95°C water bath for 5 min. Rabbit polyclonal anti-PAF1/PD2 antibody (ab20662; Abcam) and rabbit IgG were used for immunoprecipitation. For immunoblotting, the following antibodies were used: rabbit polyclonal anti-PAF1/PD2 (A300-172A, 1:5,000; Bethyl Laboratories), mouse monoclonal anti-RAD52 (sc-365341, 1:500; Santa Cruz), rabbit polyclonal anti-GFP (NB600-308, 1:1,000; Novus Biologicals), rabbit monoclonal anti-RAD51 (ab133534, 1:1,000; Abcam), rabbit monoclonal anti-total RPA32 (ab109084, 1:5,000; Abcam), rabbit polyclonal anti-phospho RPA32 (Bethyl Laboratories, A300-245A, 1:5,000), mouse monoclonal anti-CtIP (sc-271339, 1:1,000; Santa Cruz), rabbit monoclonal anti-YH2AX (Cell Signaling, 9718S, 1:1,000), rabbit polyclonal anti-cleaved caspase 3 (9661L, 1:1,000; Cell Signaling), mouse monoclonal anti-Histone H2B (sc-515808; Santa Cruz), and mouse monoclonal anti-β-actin (A5441, 1:5,000; Millipore Sigma). All antibodies were incubated overnight at 4°C. All the images related to western blot are provided in Data S1.

RNA isolation and quantitative PCR (qPCR)—RNA isolation was performed with the RNeasy Mini Kit (Qiagen) according to the manufacturer's protocol. Reverse transcription was performed using the iScript cDNA synthesis kit (Bio-Rad, 1,708,891). qPCR was performed using LightCycler 480 SYBER Green I Master mix (Roche, 04,707,516,001). All the targets were amplified (40 cycles) by utilizing gene-specific primers (Table S4) on the BioRad CFX Connect Real-Time System (BioRad). Expression levels were normalized to β-actin. See Table S4 for primer sequences.

Chromatin Fractionation—Chromatin extraction was performed following the published protocol.[78] Cells were treated with either HU, cisplatin, or gemcitabine, respectively, and after treatment, cells were cross-linked in 1% formaldehyde for 15 min. The cytosolic fraction was removed by incubation in solution A (10 mM HEPES pH 7.9, 10 mM KCl, 1.5 mM $MgCl_2$, 0.3 M sucrose, 10% glycerol, 1 mM DTT, 0.05% Triton X-100) for 10 min on ice, and centrifuged at 1500 g for 5 min at 4°C. Followed by cytoplasmic fraction isolation, the nuclear precipitate was washed and resuspended in 200 mL of solution B (3 mM EDTA, 0.2 mM EGTA, 1 mM DTT) and incubated on ice for 10 min. After incubation, the lysate was centrifuged at 2000g for 5 min at 4°C, and the nuclear supernatant was collected. The chromatin pellets were resuspended in lysis buffer (10 mM HEPES, pH 7, 500 mM NaCl, 1 mM EDTA, 1% NP-40) and sonicated at low amplitude, followed by centrifugation at 13,000 r.p.m for 1 min. For all the buffers protease-inhibitor cocktail (Roche, 50–100-3301) was added freshly before the experiment.

Chromatin immunoprecipitation (ChIP) assay—Cells were fixed with 0.4% formaldehyde, washed, harvested, and processed as mentioned by Ganguly et al.[79] with minor modifications. Cells were fixed with 0.4% formaldehyde and 1.5 mM ethylene Glycol bis (Succinimidyl succinate) (EGS; Thermofisher Scientific, #21565), washed with chilled PBS, collected, and resuspended in SDS lysis buffer (1% SDS, 10 mM EDTA, 50 mM Tris-HCl [ph 8.1], 167 mM NaCl, 1 mM PMSF, and 1 μg/mL aprotinin). Following resuspension, the samples were sonicated and diluted in ChIP dilution buffer (0.01% SDS, 1.1% Triton X-100, 1.2 mM EDTA, 16.7 mM Tris-HCl [ph8.1], 167 mM NaCl, 1 mM PMSF, and 1 μg/mL aprotinin). For input control, 10% of the sonicated samples had been separated. Immunoprecipitation was performed with ChIP-grade rabbit polyclonal anti-PAF1/PD2 antibody (Abcam, ab20662) and mouse monoclonal anti-RAD52 antibody (Santacruz, sc-365341, 1:500). Chromatin extracts were pulled down with protein G Dynabeads (ThermoFisher, 10003D). The samples were washed and eluted using ChIP DNA clean & concentrator kit (Zymo Research, D5205). The purified DNA was then subjected to PCR amplification.

Organoid culture and real-time kinetics of drug efficacy—We have used a human tumor sample to establish pancreatic and ovarian organoids. And for lung organoids, we have used tumor samples from an autochthonous mouse model (*Kras*$^{G12D+/}$, *p53*$^{R172H+/—}$, *AdCre*).[80] Tumor samples were chopped and digested enzymatically using digestion media containing collagenase II, Dispase, and 1% FBS. After digestion, the cells were embedded in Matrigel and incubated in the incubator for 15 to 20 min before adding organoids-specific media.[22,81,82]

Three independent replicates of human ovarian and pancreatic organoids and murine lung organoids were transfected with siRNA (for PAF1/PD2), followed by treatment with cisplatin or gemcitabine alone or in combination with RAD52 inhibitor D-I03. Real-time images of the organoids were captured every 3 h for 48–72 h using the IncuCyte-S5 live-cell imaging system (Sartorius). The kinetic data (organoid average growth and darkness) were analyzed and graphically represented using IncuCyte software (Sartorius). RNA was collected from organoids at the experimental endpoint to perform further analysis.

Real-time kinetics of drug efficacy on cancer Cell lines—Cells were treated with respective drugs as indicated, followed by staining the cells with IncuCyte Annexin V Orange dye (Sartorius, 4759) or Annexin V Green dye (Sartorius, 4624) for apoptosis or with IncuCyte cytotox green reagent for counting dead cells (Sartorius, 4633). Fluorescent objects were quantified in real-time to identify apoptosis or cell death via IncuCyte integrated analysis software (Sartorius). Phase-contrast images taken on the same vessels were used to quantify cell proliferation or growth using the IncuCyte cell-by-cell analysis software module (Sartorius). Real-time images of the cells were captured every 3 h for 48–72 h and were analyzed and graphically presented using IncuCyte software (Sartorius).

Colony formation assay (clonogenic assay)—In triplicates, cells were trypsinized and seeded at 1000 cells/well in a six-well plate. Cells were treated with either cisplatin or gemcitabine, as indicated. The media was changed once every three days. After 15 days of growth, the cell colonies were fixed with 100% methanol and stained with crystal violet

(0.125 gm of crystal violet in 50 mL of 20% methanol). Colonies were counted using ImageJ software.

Neutral comet assay—A neutral comet assay was performed to determine the total cellular DBSs induced by cisplatin or gemcitabine treatment. The assay was performed according to the manufacturer's protocol [Cell Biolabs, OxiSelect Comet Assay Kit (3-Well Slides), STA-351]. In brief, the cells were mixed with molten agarose before application to the comet slide. Once solidified, the embedded cells were treated with lysis buffer to relax and denature the DNA. Then the cells were electrophoresed to separate intact DNA from damaged fragments. Following electrophoresis, the samples were dried, stained with a DNA dye, and visualized under a fluorescence microscope (EVOS Cell Imaging Systems). The DNA damage was quantified by measuring the displacement between the genetic material between the 'comet head' and the 'comet tail' using ImageJ software. Around 30 images were taken per slide, and at least 50–100 cells were analyzed per sample.

Proximity ligation assay (PLA)—The *in-situ* PLA studies on HeLa cells were performed as mentioned in Duolink PLA multicolor kit (Sigma, DUO96010). Briefly, cells were fixed with 4% paraformaldehyde followed by washing with PBS, and then incubated with blocking solution for 1 h at 37°C. After blocking, primary antibodies for PAF1/PD2 (Abcam, ab20662, 1:200) and mouse monoclonal anti-RAD52 (Santacruz, sc-365341, 1:200) were added to the cells and incubated overnight at 4°C. The next day, samples were washed with 'Wash Buffer A' and then incubated with PLA probe solution for 1 h at 37°C. Following incubation with a PLA probe, the samples were washed with 'Wash Buffer A' and incubated with 1X amplification buffer for 120 min at 37°C. Subsequently, samples were washed with 'Wash Buffer B' and then mounted with DAPI-vectashield. The PLA foci were analyzed using LSM800 confocal microscope (Carl Zeiss Microimaging).

Cell-based DSB repair assay—U2OS-DR, U2OS-EJ5, and U2OS-SA were used to measure HR, NHEJ, and SSA, respectively. GFP is expressed after I-SceI-induced DSB is repaired in each DSB repair pathway. Cells were transfected with Scr or siRNA targeting PAF1/PD2 and incubated for two days. The expression plasmid of I-SceI endonuclease (a generous gift from Dr. Maria Jasin at Memorial Sloan Kettering Cancer Center) was transfected to introduce DSBs. Each DSB repair activity was determined by measuring GFP-positive cells with FACS three days after the transfection. The results (repair frequencies) were normalized to cells transfected with Scr. In parallel, the impact of the suppression of PAF1/PD2 on the expression of GFP was also measured by transfecting pEGFP plasmid encoding GFP.

Cell-cycle analysis—Cell cycle analysis was performed using propidium iodide (Roche Diagnostics) staining as per the published protocol.[83] Briefly, cells were treated with HU (4mM) for 4 h. After 4 h of treatment, cells were harvested, washed, and fixed in 70% ethanol. After fixation, the cells were left on ice for approximately 45 min, followed by centrifugation. The pellets were resuspended in Telford's reagent containing 90 mM EDTA, 2.5mU RNase A/ml, 50mg propidium iodide/ml, and 0.1% Triton X-100 in PBS. Following incubating in the ice bath for 2 h, the total DNA content was analyzed using flow cytometry.

Mass spectrometry—Mass spectrometry was performed on the PAF1/PD2-immunoprecipitates to identify the proteins that interact with PAF1/PD2. The protein fractions were excised from SDS-PAGE gel, destained, reduced with tris-carboxyethylphosphine, alkylated with iodoacetamide, and digested with sequencing-grade trypsin overnight. The tryptic peptides were analyzed using high-resolution mass spectrometry nano LC-MS/MS Tribid system, orbitrap Fusion Lumos coupled with UltiMate 3000 HPLC system (Thermofisher Scientific). 500 ng of peptides were run using the pre-column (Acclaim PepMap RSCL, 75 μm × 50 cm, nanoViper, Thermofisher Scientific), and the samples were eluted using 120-min linear gradient of CAN (5–45%) in 0.1% FA. All the MS/MS analyses were analyzed using Mascot 2.6 (Matrix Sciences), and the parameters on Mascot were set up to search the SwissProt database (Homo Sapiens). vScaffold 4.8.7 was used to determine the MS/MS-based peptide and protein identifications. At least two peptides were identified for each protein with a confidence interval >95%.

Bioinformatics analysis—Cancer Genome Atlas (TCGA) data were used to analyze the correlation between the PAF1/PD2 mRNA levels and patient survival in ovarian, lung, and pancreatic cancer. For survival analysis, patients were segregated into the top and bottom 25 percentile of PAF1/PD2 expression. TCGA was further used to analyze the relationship between the level of PAF1/PD2 and the sensitivity of cancer to chemotherapy (gemcitabine) in pancreatic cancer. Pancreatic cancer patients treated with gemcitabine as a part of first-line chemotherapy were selected from the TCGA cohort, grouped into PAF1/PD2 high and low categories based on PAF1/PD2 median expression value, and were analyzed for progressive disease/no-response and complete response. Lung adenocarcinoma (LUAD) patients were grouped into PAF1/PD2 high- and low-expression categories based on PAF1/PD2's median expression value and were analyzed for complete response and partial response versus progressive disease/stable disease.

QUANTIFICATION AND STATISTICAL ANALYSIS

Statistical analysis and graphical representations were performed using GraphPad Prism 8, except for cell and organoids real-time kinetic assays, for which the graphs were prepared using the IncuCyte software. Data are presented as mean ± standard deviation (SD). Statistical analysis of significance was calculated based on a non-paired two-tailed *Student's t-test*. A p value of <0.05 was considered statistically significant. All the *in vitro* experiments were repeated three times with biological and technical replicates. Further statistical details can be found in the figure legends.

Supplementary Material

Refer to Web version on PubMed Central for supplementary material.

ACKNOWLEDGMENTS

We very much appreciate the kind technical help of Kavita Mallya. We thank Janice A. Taylor and James R. Talaska of the Advanced Microscopy Core Facility at the University of Nebraska Medical Center for helping with confocal microscopy. The graphical abstract was created using BioRender.com. The authors were supported by grants from the National Institutes of Health (R01 CA273349, R01 CA263575, R01 CA256973, R01 CA206444, R01 CA210637, R01 CA228524, U01 CA200466, U01 CA210240, and P01 CA217798) and Nebraska Department of Health and Human Services Stem Cell Grant LB606/2022-10.

REFERENCES

1. Wang X, Zhang H, and Chen X (2019). Drug resistance and combating drug resistance in cancer. Cancer Drug Resist 2, 141–160. 10.20517/cdr.2019.10. [PubMed: 34322663]
2. Wilting RH, and Dannenberg JH (2012). Epigenetic mechanisms in tumorigenesis, tumor cell heterogeneity and drug resistance. Drug Resist. Updat 15, 21–38. 10.1016/j.drup.2012.01.008. [PubMed: 22356866]
3. Mansoori B, Mohammadi A, Davudian S, Shirjang S, and Baradaran B (2017). The different mechanisms of cancer drug resistance: a brief review. Adv. Pharm. Bull 7, 339–348. 10.15171/apb.2017.041. [PubMed: 29071215]
4. Peng Q, Weng K, Li S, Xu R, Wang Y, and Wu Y (2021). A perspective of epigenetic regulation in radiotherapy. Front. Cell Dev. Biol 9, 624312. 10.3389/fcell.2021.624312. [PubMed: 33681204]
5. Fernandez A, O'Leary C, O'Byrne KJ, Burgess J, Richard DJ, and Suraweera A (2021). Epigenetic mechanisms in DNA double strand break repair: a clinical review. Front. Mol. Biosci 8, 685440. 10.3389/fmolb.2021.685440. [PubMed: 34307454]
6. Shin MH, He Y, Marrogi E, Piperdi S, Ren L, Khanna C, Gorlick R, Liu C, and Huang J (2016). A RUNX2-mediated epigenetic regulation of the survival of p53 defective cancer cells. PLoS Genet 12, e1005884. 10.1371/journal.pgen.1005884. [PubMed: 26925584]
7. Li L, Schaid DJ, Fridley BL, Kalari KR, Jenkins GD, Abo RP, Batzler A, Moon I, Pelleymounter L, Eckloff BW, et al. (2012). Gemcitabine metabolic pathway genetic polymorphisms and response in patients with non-small cell lung cancer. Pharmacogenet. Genomics 22, 105–116. 10.1097/FPC.0b013e32834dd7e2. [PubMed: 22173087]
8. Wang L, Zhao X, Fu J, Xu W, and Yuan J (2021). The role of tumour metabolism in cisplatin resistance. Front. Mol. Biosci 8, 691795. 10.3389/fmolb.2021.691795. [PubMed: 34250022]
9. Galanski M (2006). Recent developments in the field of anticancer platinum complexes. Recent Pat. Anti-Cancer Drug Discov 1, 285–295. 10.2174/157489206777442287.
10. de Sousa Cavalcante L, and Monteiro G (2014). Gemcitabine: metabolism and molecular mechanisms of action, sensitivity and chemoresistance in pancreatic cancer. Eur. J. Pharmacol 741, 8–16. 10.1016/j.ejphar.2014.07.041. [PubMed: 25084222]
11. Christensen S, Van der Roest B, Besselink N, Janssen R, Boymans S, Martens JWM, Yaspo ML, Priestley P, Kuijk E, Cuppen E, and Van Hoeck A (2019). 5-Fluorouracil treatment induces characteristic T>G mutations in human cancer. Nat. Commun 10, 4571. 10.1038/s41467-019-12594-8. [PubMed: 31594944]
12. Siddik ZH (2003). Cisplatin: mode of cytotoxic action and molecular basis of resistance. Oncogene 22, 7265–7279. 10.1038/sj.onc.1206933. [PubMed: 14576837]
13. Binenbaum Y, Na'ara S, and Gil Z (2015). Gemcitabine resistance in pancreatic ductal adenocarcinoma. Drug Resist. Updat 23, 55–68. 10.1016/j.drup.2015.10.002. [PubMed: 26690340]
14. Shukla SK, Purohit V, Mehla K, Gunda V, Chaika NV, Vernucci E, King RJ, Abrego J, Goode GD, Dasgupta A, et al. (2017). MUC1 and HIF-1alpha signaling crosstalk induces anabolic glucose metabolism to impart gemcitabine resistance to pancreatic cancer. Cancer Cell 32, 71–87.e7 10.1016/j.ccell.2017.06.004. [PubMed: 28697344]
15. Shen DW, Pouliot LM, Hall MD, and Gottesman MM (2012). Cisplatin resistance: a cellular self-defense mechanism resulting from multiple epigenetic and genetic changes. Pharmacol. Rev 64, 706–721. 10.1124/pr.111.005637. [PubMed: 22659329]
16. Huang D, Duan H, Huang H, Tong X, Han Y, Ru G, Qu L, Shou C, and Zhao Z (2016). Cisplatin resistance in gastric cancer cells is associated with HER2 upregulation-induced epithelial-mesenchymal transition. Sci. Rep 6, 20502. 10.1038/srep20502. [PubMed: 26846307]
17. Du P, Wang Y, Chen L, Gan Y, and Wu Q (2016). High ERCC1 expression is associated with platinum-resistance, but not survival in patients with epithelial ovarian cancer. Oncol. Lett 12, 857–862. 10.3892/ol.2016.4732. [PubMed: 27446360]
18. Metzger R, Leichman CG, Danenberg KD, Danenberg PV, Lenz HJ, Hayashi K, Groshen S, Salonga D, Cohen H, Laine L, et al. (1998). ERCC1 mRNA levels complement thymidylate synthase mRNA levels in predicting response and survival for gastric cancer patients receiving

combination cisplatin and fluorouracil chemotherapy. J. Clin. Oncol 16, 309–316. 10.1200/jco.1998.16.1.309. [PubMed: 9440758]

19. Fijo1ek J, Wiatr E, Rowińska-Zakrzewska E, Giedronowicz D, Langfort R, Chabowski M, Or1owski T, and Roszkowski K (2006). p53 and HER2/neu expression in relation to chemotherapy response in patients with non-small cell lung cancer. Int. J. Biol. Markers 21, 81–87. [PubMed: 16847810]
20. Prudner BC, Rathore R, Robinson AM, Godec A, Chang SF, Hawkins WG, Hirbe AC, and Van Tine BA (2019). Arginine starvation and docetaxel induce c-Myc-driven hENT1 surface expression to overcome gemcitabine resistance in ASS1-negative tumors. Clin. Cancer Res 25, 5122–5134. 10.1158/1078-0432.Ccr-19-0206. [PubMed: 31113844]
21. Rauth S, Karmakar S, Shah A, Seshacharyulu P, Nimmakayala RK, Ganguly K, Bhatia R, Muniyan S, Kumar S, Dutta S, et al. (2021). SUMO modification of PAF1/PD2 enables PML interaction and promotes radiation resistance in pancreatic ductal adenocarcinoma. Mol. Cell Biol 41, e0013521. 10.1128/mcb.00135-21. [PubMed: 34570619]
22. Karmakar S, Rauth S, Nallasamy P, Perumal N, Nimmakayala RK, Leon F, Gupta R, Barkeer S, Venkata RC, Raman V, et al. (2020). RNA polymerase II-associated factor 1 regulates stem cell features of pancreatic cancer cells, independently of the PAF1 complex, via interactions with PHF5A and DDX3. Gastroenterology 159, 1898–1915.e6 10.1053/j.gastro.2020.07.053. [PubMed: 32781084]
23. Nimmakayala RK, Seshacharyulu P, Lakshmanan I, Rachagani S, Chugh S, Karmakar S, Rauth S, Vengoji R, Atri P, Talmon GA, et al. (2018). Cigarette smoke induces stem cell features of pancreatic cancer cells via PAF1. Gastroenterology 155, 892–908.e6 10.1053/j.gastro.2018.05.041. [PubMed: 29864419]
24. Karmakar S, Seshacharyulu P, Lakshmanan I, Vaz AP, Chugh S, Sheinin YM, Mahapatra S, Batra SK, and Ponnusamy MP (2017). hPaf1/PD2 interacts with OCT3/4 to promote self-renewal of ovarian cancer stem cells. Oncotarget 8, 14806–14820. 10.18632/on-cotarget.14775. [PubMed: 28122356]
25. Dey P, Rachagani S, Vaz AP, Ponnusamy MP, and Batra SK (2014). PD2/Paf1 depletion in pancreatic acinar cells promotes acinar-to-ductal metaplasia. Oncotarget 5, 4480–4491. 10.18632/oncotar-get.2041. [PubMed: 24947474]
26. Zhi X, Giroux-Leprieur E, Wislez M, Hu M, Zhang Y, Shi H, Du K, and Wang L (2015). Human RNA polymerase II associated factor 1 complex promotes tumorigenesis by activating c-MYC transcription in non-small cell lung cancer. Biochem. Biophys. Res. Commun 465, 685–690. 10.1016/j.bbrc.2015.08.017. [PubMed: 26282204]
27. Hetzner K, Garcia-Cuellar MP, Büttner C, and Slany RK (2018). The interaction of ENL with PAF1 mitigates polycomb silencing and facilitates murine leukemogenesis. Blood 131, 662–673. 10.1182/blood-2017-11-815035. [PubMed: 29217648]
28. Zheng JJ, He Y, Liu Y, Li FS, Cui Z, Du XM, Wang CP, and Wu YM (2020). Novel role of PAF1 in attenuating radiosensitivity in cervical cancer by inhibiting IER5 transcription. Radiat. Oncol 15, 131. 10.1186/s13014-020-01580-w. [PubMed: 32471508]
29. Vaz AP, Ponnusamy MP, Rachagani S, Dey P, Ganti AK, and Batra SK (2014). Novel role of pancreatic differentiation 2 in facilitating self-renewal and drug resistance of pancreatic cancer stem cells. Br. J. Cancer 111, 486–496. 10.1038/bjc.2014.152. [PubMed: 25003666]
30. Xie M, Zhang L, He CS, Xu F, Liu JL, Hu ZH, Zhao LP, and Tian Y (2012). Activation of Notch-1 enhances epithelial-mesenchymal transition in gefitinib-acquired resistant lung cancer cells. J. Cell. Biochem 113, 1501–1513. 10.1002/jcb.24019. [PubMed: 22173954]
31. Wang Z, Li Y, Kong D, Banerjee S, Ahmad A, Azmi AS, Ali S, Abbruzzese JL, Gallick GE, and Sarkar FH (2009). Acquisition of epithelial-mesenchymal transition phenotype of gemcitabine-resistant pancreatic cancer cells is linked with activation of the notch signaling pathway. Cancer Res 69, 2400–2407. 10.1158/0008-5472.Can-08-4312. [PubMed: 19276344]
32. Huo H, Magro PG, Pietsch EC, Patel BB, and Scotto KW (2010). Histone methyltransferase MLL1 regulates MDR1 transcription and chemoresistance. Cancer Res 70, 8726–8735. 10.1158/0008-5472.Can-10-0755. [PubMed: 20861184]

33. Dey P, Ponnusamy MP, Deb S, and Batra SK (2011). Human RNA polymerase II-association factor 1 (hPaf1/PD2) regulates histone methylation and chromatin remodeling in pancreatic cancer. PLoS One 6, e26926. 10.1371/journal.pone.0026926. [PubMed: 22046413]
34. Rauth S, Karmakar S, Batra SK, and Ponnusamy MP (2021). Recent advances in organoid development and applications in disease modeling. Biochim. Biophys. Acta. Rev. Cancer 1875, 188527. 10.1016/j.bbcan.2021.188527. [PubMed: 33640383]
35. Carley AC, Jalan M, Subramanyam S, Roy R, Borgstahl GEO, and Powell SN (2022). RPA phosphorylation facilitates RAD52 dependent homologous recombination in BRCA-deficient cells. Mol. Cell Biol 42, mcb0052421. 10.1128/mcb.00524-21.
36. Rossi MJ, DiDomenico SF, Patel M, and Mazin AV (2021). RAD52: paradigm of synthetic lethality and new developments. Front. Genet 12, 780293. 10.3389/fgene.2021.780293. [PubMed: 34887904]
37. Tan J, Duan M, Yadav T, Phoon L, Wang X, Zhang JM, Zou L, and Lan L (2020). An R-loop-initiated CSB-RAD52-POLD3 pathway suppresses ROS-induced telomeric DNA breaks. Nucleic Acids Res 48, 1285–1300. 10.1093/nar/gkz1114. [PubMed: 31777915]
38. Yasuhara T, Kato R, Hagiwara Y, Shiotani B, Yamauchi M, Nakada S, Shibata A, and Miyagawa K (2018). Human Rad52 promotes XPG-mediated R-loop processing to initiate transcription-associated homologous recombination repair. Cell 175, 558–570.e11 10.1016/j.cell.2018.08.056. [PubMed: 30245011]
39. Bhowmick R, Minocherhomji S, and Hickson ID (2016). RAD52 facilitates mitotic DNA synthesis following replication stress. Mol. Cell 64, 1117–1126. 10.1016/j.molcel.2016.10.037. [PubMed: 27984745]
40. Wu X (2019). Replication stress response links RAD52 to protecting common fragile sites. Cancers 11, 1467. 10.3390/cancers11101467. [PubMed: 31569559]
41. Patel PS, Algouneh A, and Hakem R (2021). Exploiting synthetic lethality to target BRCA1/2-deficient tumors: where we stand. Oncogene 40, 3001–3014. 10.1038/s41388-021-01744-2. [PubMed: 33716297]
42. Kelso AA, Lopezcolorado FW, Bhargava R, and Stark JM (2019). Distinct roles of RAD52 and POLQ in chromosomal break repair and replication stress response. PLoS Genet 15, e1008319. 10.1371/journal.pgen.1008319. [PubMed: 31381562]
43. Shi TY, Yang G, Tu XY, Yang JM, Qian J, Wu XH, Zhou XY, Cheng X, and Wei Q (2012). RAD52 variants predict platinum resistance and prognosis of cervical cancer. PLoS One 7, e50461. 10.1371/journal.pone.0050461. [PubMed: 23209746]
44. Rottenberg S, Disler C, and Perego P (2021). The rediscovery of platinum-based cancer therapy. Nat. Rev. Cancer 21, 37–50. 10.1038/s41568-020-00308-y. [PubMed: 33128031]
45. Li LY, Guan YD, Chen XS, Yang JM, and Cheng Y (2020). DNA repair pathways in cancer therapy and resistance. Front. Pharmacol 11, 629266. 10.3389/fphar.2020.629266. [PubMed: 33628188]
46. Xu R, Yu S, Zhu D, Huang X, Xu Y, Lao Y, Tian Y, Zhang J, Tang Z, Zhang Z, et al. (2019). hCINAP regulates the DNA-damage response and mediates the resistance of acute myelocytic leukemia cells to therapy. Nat. Commun 10, 3812. 10.1038/s41467-019-11795-5. [PubMed: 31444354]
47. Liew LP, Lim ZY, Cohen M, Kong Z, Marjavaara L, Chabes A, and Bell SD (2016). Hydroxyurea-mediated cytotoxicity without inhibition of ribonucleotide reductase. Cell Rep 17, 1657–1670. 10.1016/j.celrep.2016.10.024. [PubMed: 27806303]
48. Bétous R, Goullet de Rugy T, Pelegrini AL, Queille S, de Villartay JP, and Hoffmann JS (2018). DNA replication stress triggers rapid DNA replication fork breakage by Artemis and XPF. PLoS Genet 14, e1007541. 10.1371/journal.pgen.1007541. [PubMed: 30059501]
49. Gunn A, and Stark JM (2012). I-SceI-based assays to examine distinct repair outcomes of mammalian chromosomal double strand breaks. Methods Mol. Biol 920, 379–391. 10.1007/978-1-61779-998-3_27. [PubMed: 22941618]
50. Lisby M, Rothstein R, and Mortensen UH (2001). Rad52 forms DNA repair and recombination centers during S phase. Proc. Natl. Acad. Sci. USA 98, 8276–8282. 10.1073/pnas.121006298. [PubMed: 11459964]

51. Hengel SR, Spies MA, and Spies M (2017). Small-molecule inhibitors targeting DNA repair and DNA repair deficiency in research and cancer therapy. Cell Chem. Biol 24, 1101–1119. 10.1016/j.chembiol.2017.08.027. [PubMed: 28938088]
52. Al-Mugotir M, Lovelace JJ, George J, Bessho M, Pal D, Struble L, Kolar C, Rana S, Natarajan A, Bessho T, and Borgstahl GEO (2021). Selective killing of homologous recombination-deficient cancer cell lines by inhibitors of the RPA:RAD52 protein-protein interaction. PLoS One 16, e0248941. 10.1371/journal.pone.0248941. [PubMed: 33784323]
53. Bertotti A, and Sassi F (2015). Molecular pathways: sensitivity and resistance to anti-EGFR antibodies. Clin. Cancer Res 21, 3377–3383. 10.1158/1078-0432.Ccr-14-0848. [PubMed: 26071484]
54. Makovec T (2019). Cisplatin and beyond: molecular mechanisms of action and drug resistance development in cancer chemotherapy. Radiol. Oncol 53, 148–158. 10.2478/raon-2019-0018. [PubMed: 30956230]
55. Kara A, Özgür A, Nalbantoğlu S, and Karadağ A (2021). DNA repair pathways and their roles in drug resistance for lung adenocarcinoma. Mol. Biol. Rep 48, 3813–3825. 10.1007/s11033-021-06314-z. [PubMed: 33856604]
56. Zhou Y, Zheng M, Liu Z, Yang H, Zhu P, Jiang JL, Tang J, and Chen ZN (2020). CD147 promotes DNA damage response and gemcitabine resistance via targeting ATM/ATR/p53 and affects prognosis in pancreatic cancer. Biochem. Biophys. Res. Commun 528, 62–70. 10.1016/j.bbrc.2020.05.005. [PubMed: 32456796]
57. Tatum D, Li W, Placer M, and Li S (2011). Diverse roles of RNA polymerase II-associated factor 1 complex in different subpathways of nucleotide excision repair. J. Biol. Chem 286, 30304–30313. 10.1074/jbc.M111.252981. [PubMed: 21737840]
58. Gothwal SK, Patel NJ, Colletti MM, Sasanuma H, Shinohara M, Hochwagen A, and Shinohara A (2016). The double-strand break landscape of meiotic chromosomes is shaped by the Paf1 transcription elongation complex in Saccharomyces cerevisiae. Genetics 202, 497–512. 10.1534/genetics.115.177287. [PubMed: 26627841]
59. van den Heuvel D, Spruijt CG, González-Prieto R, Kragten A, Paulsen MT, Zhou D, Wu H, Apelt K, van der Weegen Y, Yang K, et al. (2021). A CSB-PAF1C axis restores processive transcription elongation after DNA damage repair. Nat. Commun 12, 1342. 10.1038/s41467-021-21520-w. [PubMed: 33637760]
60. Kokic G, Wagner FR, Chernev A, Urlaub H, and Cramer P (2021). Structural basis of human transcription-DNA repair coupling. Nature 598, 368–372. 10.1038/s41586-021-03906-4. [PubMed: 34526721]
61. Tiwari V, Kulikowicz T, Wilson DM 3rd, and Bohr VA (2021). LEO1 is a partner for Cockayne syndrome protein B (CSB) in response to transcription-blocking DNA damage. Nucleic Acids Res 49, 6331–6346. 10.1093/nar/gkab458. [PubMed: 34096589]
62. Shivji MKK, Renaudin X, Williams ÇH, and Venkitaraman AR (2018). BRCA2 regulates transcription elongation by RNA polymerase II to prevent R-loop accumulation. Cell Rep 22, 1031–1039. 10.1016/j.celrep.2017.12.086. [PubMed: 29386125]
63. Wang H, Li S, Oaks J, Ren J, Li L, and Wu X (2018). The concerted roles of FANCM and Rad52 in the protection of common fragile sites. Nat. Commun 9, 2791. 10.1038/s41467-018-05066-y. [PubMed: 30022024]
64. Nogueira A, Fernandes M, Catarino R, and Medeiros R (2019). RAD52 functions in homologous recombination and its importance on genomic integrity maintenance and cancer therapy. Cancers 11, 1622. 10.3390/cancers11111622. [PubMed: 31652722]
65. Hamimes S, Arakawa H, Stasiak AZ, Kierzek AM, Hirano S, Yang YG, Takata M, Stasiak A, Buerstedde JM, and Van Dyck E (2005). RDM1, a novel RNA recognition motif (RRM)-containing protein involved in the cell response to cisplatin in vertebrates. J. Biol. Chem 280, 9225–9235. 10.1074/jbc.M412874200. [PubMed: 15611051]
66. Li HM, Yuan P, Yu DK, Ma F, Tan WW, Feng T, Yang J, Huang Y, Lin DX, Xu BH, and Tan W (2016). [Genetic variation in DNA repair gene RAD52 is associated with the response to platinum-based chemotherapy in SCLC patients]. Zhonghua Zhongliu Zazhi 38, 504–509. 10.3760/cma.j.issn.0253-3766.2016.07.005. [PubMed: 27531263]

67. Lieberman R, and You M (2017). Corrupting the DNA damage response: a critical role for Rad52 in tumor cell survival. Aging (Albany NY) 9, 1647–1659. 10.18632/aging.101263. [PubMed: 28722656]
68. Han S, Gao F, Yang W, Ren Y, Liang X, Xiong X, Pan W, Zhou L, Zhou C, Ma F, and Yang M (2015). Identification of an SCLC susceptibility rs7963551 genetic polymorphism in a previously GWAS-identified 12p13.33 RAD52 lung cancer risk locus in the Chinese population. Int. J. Clin. Exp. Med 8, 16528–16535. [PubMed: 26629180]
69. Baumann P, and West SC (1998). Role of the human RAD51 protein in homologous recombination and double-stranded-break repair. Trends Biochem. Sci 23, 247–251. 10.1016/s0968-0004(98)01232-8. [PubMed: 9697414]
70. Buis J, Stoneham T, Spehalski E, and Ferguson DO (2012). Mre11 regulates CtIP-dependent double-strand break repair by interaction with CDK2. Nat. Struct. Mol. Biol 19, 246–252. 10.1038/nsmb.2212. [PubMed: 22231403]
71. Symington LS (2016). Mechanism and regulation of DNA end resection in eukaryotes. Crit. Rev. Biochem. Mol. Biol 51, 195–212. 10.3109/10409238.2016.1172552. [PubMed: 27098756]
72. Zhou W, Yao Y, Scott AJ, Wilder-Romans K, Dresser JJ, Werner CK, Sun H, Pratt D, Sajjakulnukit P, Zhao SG, et al. (2020). Purine metabolism regulates DNA repair and therapy resistance in glioblastoma. Nat. Commun 11, 3811. 10.1038/s41467-020-17512-x. [PubMed: 32732914]
73. Turgeon MO, Perry NJS, and Poulogiannis G (2018). DNA damage, repair, and cancer metabolism. Front. Oncol 8, 15. 10.3389/fonc.2018.00015. [PubMed: 29459886]
74. Dibitetto D, Sims JR, Ascenção CFR, Feng K, Kim D, Oberly S, Freire R, and Smolka MB (2020). Intrinsic ATR signaling shapes DNA end resection and suppresses toxic DNA-PKcs signaling. NAR Cancer 2, zcaa006. 10.1093/narcan/zcaa006. [PubMed: 32743550]
75. Schettini F, Giudici F, Bernocchi O, Sirico M, Corona SP, Giuliano M, Locci M, Paris I, Scambia G, De Placido S, et al. (2021). Poly (ADP-ribose) polymerase inhibitors in solid tumours: systematic review and meta-analysis. Eur. J. Cancer 149, 134–152. 10.1016/j.ejca.2021.02.035. [PubMed: 33862496]
76. Dekkers JF, van Vliet EJ, Sachs N, Rosenbluth JM, Kopper O, Rebel HG, Wehrens EJ, Piani C, Visvader JE, Verissimo CS, et al. (2021). Long-term culture, genetic manipulation and xenotransplantation of human normal and breast cancer organoids. Nat. Protoc 16, 1936–1965. 10.1038/s41596-020-00474-1. [PubMed: 33692550]
77. Chou TC (2010). Drug combination studies and their synergy quantification using the Chou-Talalay method. Cancer Res 70, 440–446. 10.1158/0008-5472.Can-09-1947. [PubMed: 20068163]
78. Ochs F, Somyajit K, Altmeyer M, Rask MB, Lukas J, and Lukas C (2016). 53BP1 fosters fidelity of homology-directed DNA repair. Nat. Struct. Mol. Biol 23, 714–721. 10.1038/nsmb.3251. [PubMed: 27348077]
79. Ganguly K, Bhatia R, Rauth S, Kisling A, Atri P, Thompson C, Vengoji R, Ram Krishn S, Shinde D, Thomas V, et al. (2022). Mucin 5AC serves as the nexus for β-Catenin/c-Myc interplay to promote glutamine dependency during pancreatic cancer chemoresistance. Gastroenterology 162, 253–268.e13 10.1053/j.gastro.2021.09.017. [PubMed: 34534538]
80. Lakshmanan I, Rachagani S, Hauke R, Krishn SR, Paknikar S, Seshacharyulu P, Karmakar S, Nimmakayala RK, Kaushik G, Johansson SL, et al. (2016). MUC5AC interactions with integrin b4 enhances the migration of lung cancer cells through FAK signaling. Oncogene 35, 4112–4121. 10.1038/onc.2015.478. [PubMed: 26751774]
81. Nanki Y, Chiyoda T, Hirasawa A, Ookubo A, Itoh M, Ueno M, Akahane T, Kameyama K, Yamagami W, Kataoka F, and Aoki D (2020). Patient-derived ovarian cancer organoids capture the genomic profiles of primary tumours applicable for drug sensitivity and resistance testing. Sci. Rep 10, 12581. 10.1038/s41598-020-69488-9. [PubMed: 32724113]
82. Kaushik G, Ponnusamy MP, and Batra SK (2018). Concise review: current status of three-dimensional organoids as preclinical models. Stem Cell 36, 1329–1340. 10.1002/stem.2852.
83. Lakshmanan I, Ponnusamy MP, Das S, Chakraborty S, Haridas D, Mukhopadhyay P, Lele SM, and Batra SK (2012). MUC16 induced rapid G2/M transition via interactions with JAK2 for increased proliferation and anti-apoptosis in breast cancer cells. Oncogene 31, 805–817. 10.1038/onc.2011.297. [PubMed: 21785467]

Highlights

- Chemoresistance in ovarian, lung, and pancreatic cancers links to increased expression of PAF1
- PAF1 upregulates chemoresistance- and DNA-repair activity in chemoresistance cells
- PAF1 interacts with and regulates RAD52 DNA-repair activity
- Targeting RAD52 and PAF1 can sensitize chemoresistance cells to chemotherapies

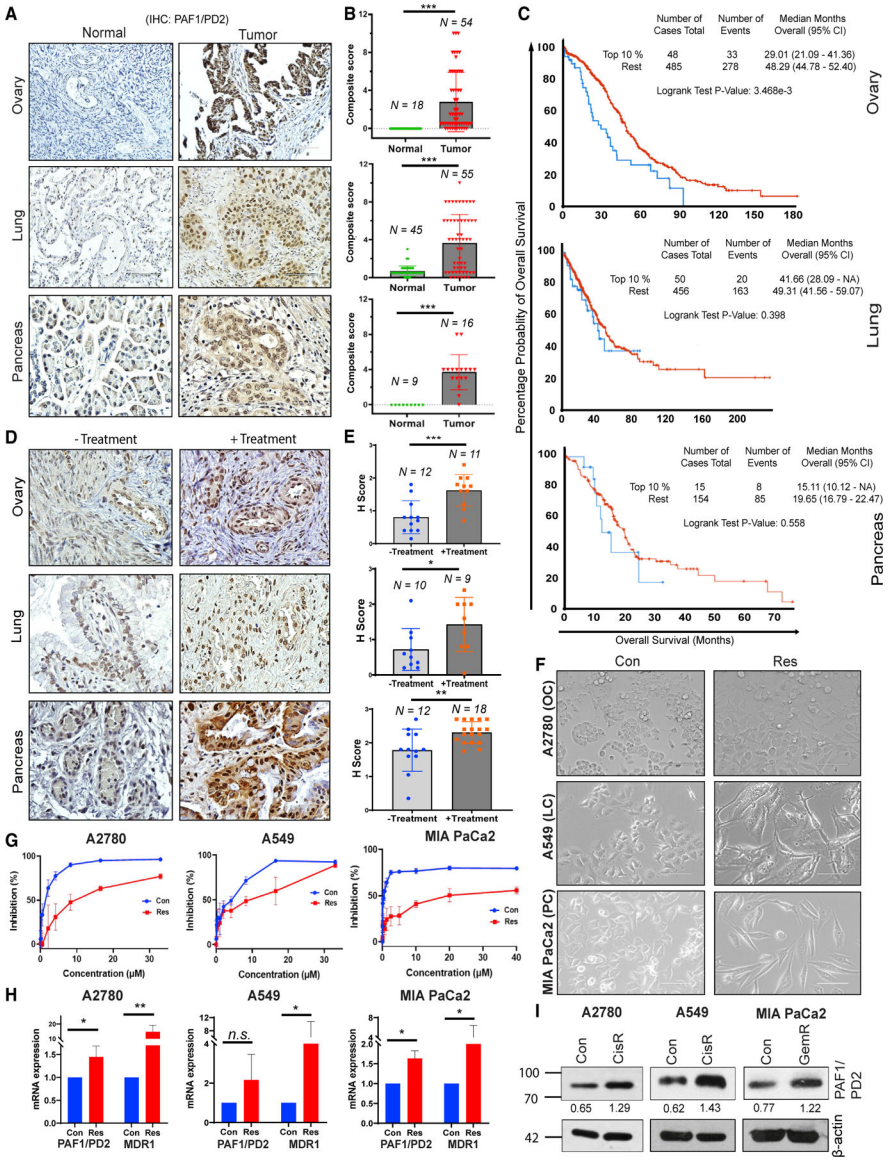

Figure 1. Elevated expression of PAF1/PD2 is associated with chemotherapy resistance in ovarian, lung, and pancreatic cancers

(A) Representative immunohistochemical (IHC) staining images of PAF1/PD2 in primary tumor and normal tissues from ovarian, lung, and pancreatic cancer patients. Scale bar, 200 μm.

(B) Graphs correspond to the quantification of PAF1/PD2 in the indicated tumor type, represented by composite score. *N* represents the number of patient samples in each group. Data are presented as mean ± SD.

(C) Kaplan-Meier survival analysis of ovarian, lung, and PDAC patients showed that the top 10% of patients with high expression of PAF1/PD2 (~2-fold) is associated with poor survival.

(D) Representative IHC images of PAF1/PD2 in treatment-naive (−Treatment) and chemotherapy-treated (+Treatment) patients' samples. Scale bar, 200 μm.

(E) Graphs correspond to the quantification of PAF1/PD2 in the indicated group represented by H-score. Data are presented as mean ± SD, and *N* represents the number of samples in each group.

(F) Bright field images of A2780, A549, and MIA PaC2 cells and their corresponding chemotherapy-resistant cells. Scale bars, 100 μm.

(G) The sensitivity of control (WT) cells with the CisR or GemR cells is determined by MTT cytotoxicity assays after 48 h of cisplatin or gemcitabine treatment. Data are represented as mean ± SD; n = 3.

(H) Relative mRNA expression of PAF1/PD2 in CisR or GemR cells versus their control cells. Data are represented as mean ± SD; n = 3.

(I) Immunoblotting analysis shows the expression of PAF1/PD2 in control versus CisR or GemR cells. Relative densitometric values are provided below the blot images after normalizing to β-actin.

Student's t test compared the bar charts in (B), (E), and (H). Survival in (C) was compared by log rank (Mantel-Cox) test. *$p < 0.05$, **$p < 0.01$, ***$p < 0.001$. LC, lung cancer; n.s., non-significant; OC, ovarian cancer; PC, pancreatic cancer. See also Tables S1 and S2.

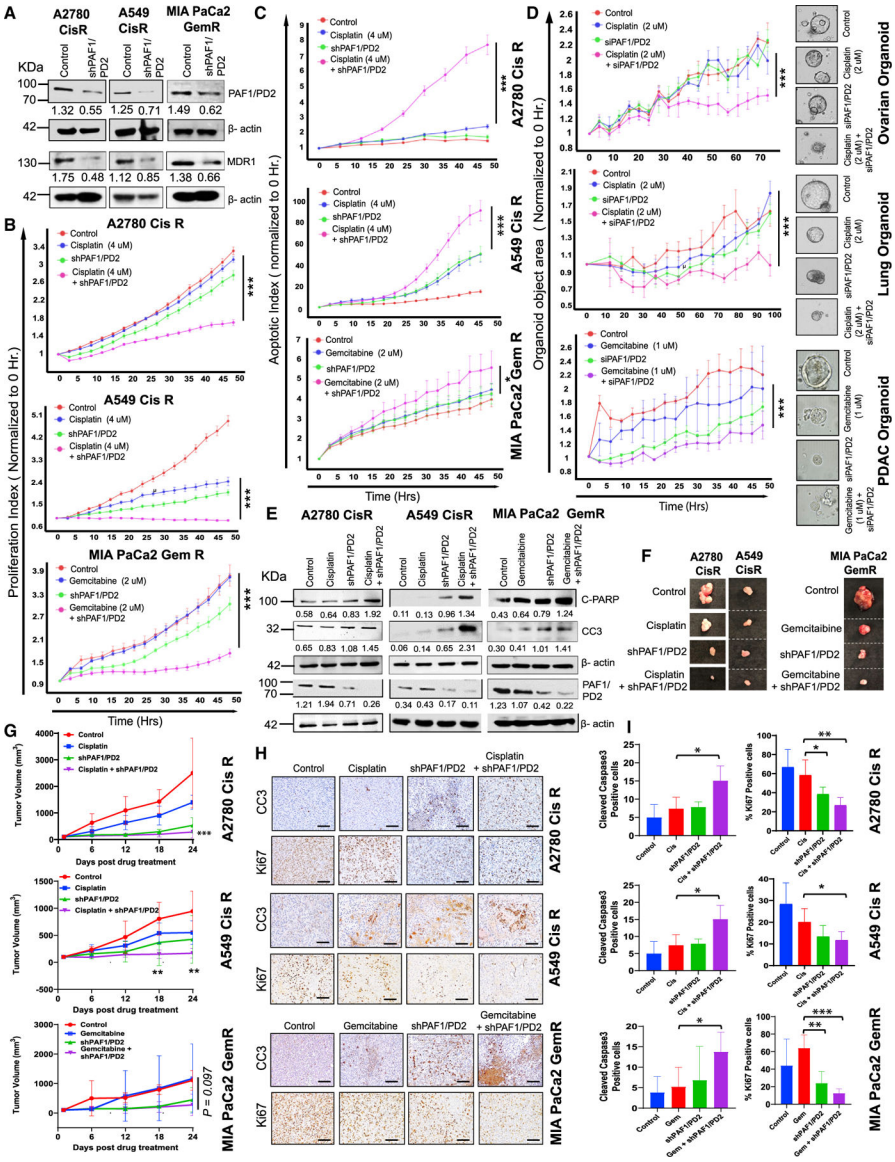

Figure 2. Knocking down PAF1/PD2 increases chemotherapy sensitivity in CisR and GemR cells

(A) Immunoblotting analysis showing the PAF1/PD2 knockdown and MDR1 expression in indicated cells. β-Actin was used as a loading control. Relative densitometric values are provided below the blot images after normalizing to β-actin.

(B) Incucyte Cell-by-Cell analysis demonstrating a time-dependent decrease in proliferation of chemoresistant cells on treatment with either cisplatin (4 μM) or gemcitabine (2 μM) along with PAF1/PD2 knockdown.

(C) Luminescence assay (Annexin V activation) demonstrating the time-dependent increase in apoptosis of chemoresistant cells treated with cisplatin (4 μM) or gemcitabine (2 μM) combined with PAF1/PD2 knockdown. For both graphs in (B) and (C), 3,000 cells/well were seeded as described in the star methods, and four 10× images per well were taken every 3 h for 48 h. Data are presented as mean ± SEM; n = 3.

(D) Incucyte-based real-time kinetics of organoids growth (presented as organoid object area) depicting reduced growth of tumor organoids with PAF1/PD2 knockdown and cisplatin (2 μM)/gemcitabine (1 μM) treatment. One 4× image per well is taken every 3 h, and data are presented as mean ± SEM; n = 3. Representative images of the corresponding organoids were presented on the left side of the graph, collected with the Incucyte System. Scale bar, 1,000 μm.

(E) Cleaved PARP (C-PARP), Cleaved Caspase-3 (CC3), and PAF1/PD2 expression were detected by western blot in the indicated cells on treatment with cisplatin (4 μM) or gemcitabine (2 μM) alone and PAF1/PD2 knockdown alone or in the combination of PAF1/PD2 knockdown with chemotherapy. β-Actin was used as a loading control. Relative densitometric values are provided below the blot images after normalizing to β-actin.

(F–I) Effect of PAF1/PD2 knockdown on cisplatin or gemcitabine responsiveness in xenograft mice (n = 3). Representative tumor images on necropsy in subcutaneously implanted mice subjected to treatments with control, cisplatin (5 mg/kg of body weight; twice a week), or gemcitabine (12.5 mg/kg of body weight; once a week) alone; PAF1/PD2 knockdown alone; or PAF1/PD2 knockdown with cisplatin or gemcitabine (F). Tumor volumes of mice with the indicated treatments (G). Representative images of IHC staining (H) and quantification (I) of Ki67 and CC3 in the formalin-fixed tumor sections from the indicated treatment groups. Pathologists quantified % Ki67-positive cells, and CC3-positive cells were counted manually in five fields of five to six tumors of each group.

For G and I, data are presented as mean ± SD. In all graphs, the group treated with a combination of PAF1/PD2 knockdown along with cisplatin or gemcitabine was compared with the respective group that was treated with cisplatin or gemcitabine alone by non-parametric Student’s t test. Scale bars, 250 μm (H). *$p < 0.05$, **$p < 0.01$, ***$p < 0.001$.

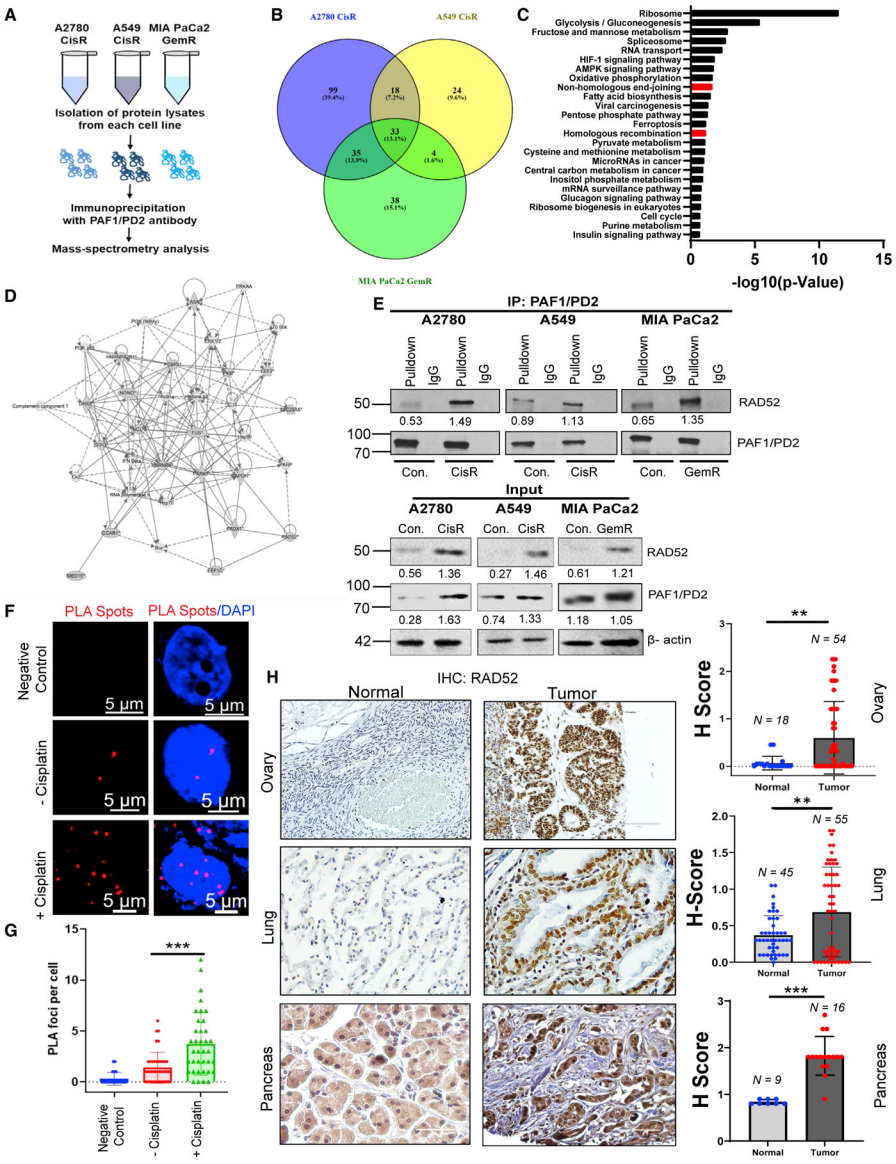

Figure 3. PAF1/PD2 physically associates with RAD52

(A) Schematic diagram showing that protein lysate was collected from indicated cells, and immunoprecipitation (IP) was performed using PAF1/PD2 antibody. The IP product was given for mass spectrometry analysis.

(B) Protein interactomes from the different cell lines were analyzed. Venn diagram showing the overlapping number of candidates among all three cell lines.

(C) Pathway enrichment analysis of the common interacting proteins showing the enrichment of pathways involved in DNA double-strand break (DSB) repair.

(D) Ingenuity systems-generated pathway of PAF1/PD2 interacting proteins (overlapping candidates) following mass spectrometry. Solid or dashed lines demonstrate direct or indirect interactions, respectively.

(E) Validation of PAF1/PD2 interaction with RAD52 in control and cisplatin or gemcitabine resistance cells using IP. Immunoblot images with IP data represent the densitometric values

of RAD52 after normalizing to PAF1/PD2, and for the Input immunoblot images, the densitometric values for PAF1 and RAD52 are normalized to β-actin.

(F and G) Analysis of PAF1/PD2-RAD52 interaction by *in situ* PLA assay in HeLa cells following cisplatin treatment. Negative control was subjected to PLA with anti-PAF1/PD2 antibody only. Representative images (F) and quantitation (G) of the PLA foci (red dots). Scale bars, 5 μm. Values are presented as mean ± SD. n ≥ 30 cells. ***p < 0.001.

(H) IHC staining of the same tissue array used in Figure 1A, with the left panel showing the representative images of RAD52 staining in indicated samples. Scale bars, 200 μm. The right panel represents the H-score for RAD52 staining in indicated samples. *N* represents the number of patient samples in each group. Data are presented as mean ± SD. *p < 0.05, **p < 0.01, ***p < 0.001. See also Table S5.

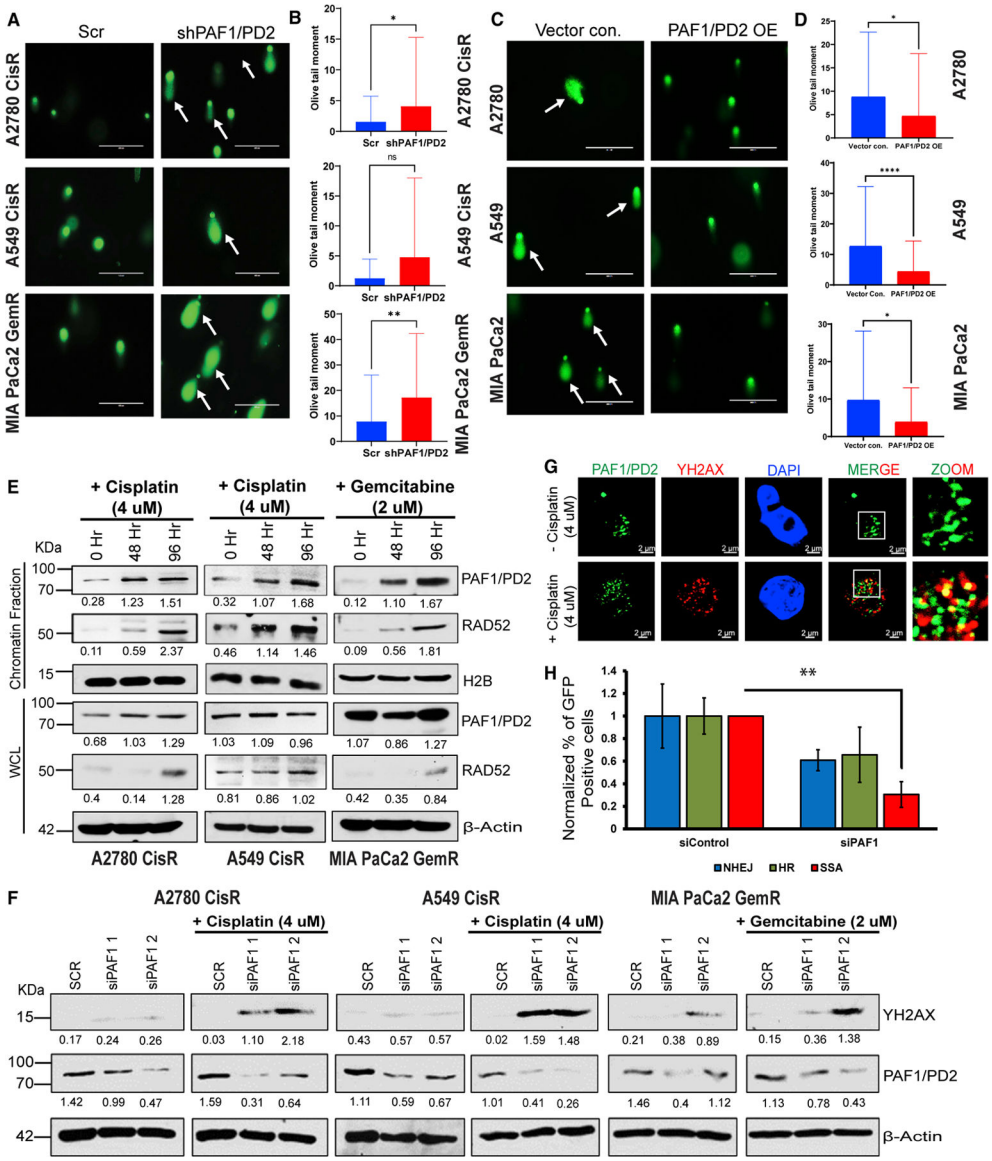

Figure 4. PAF1/PD2 is associated with DNA repair

(A and B) Scr and PAF1/PD2 knockdown cells were treated with cisplatin (4 μM) or gemcitabine (2 μM), respectively, and subjected to neutral comet assay. Representative images (A) and the quantitation of tail moments (B) illustrate that knocking down PAF1/PD2 increases the total DNA damage in cells.

(C and D) Vector control and PAF1/PD2-overexpressing cells were treated with cisplatin (4 μM) or gemcitabine (2 μM), respectively, followed by neutral comet assay. Representative images (C) and the bar graph represent tail moments' quantitation (D). For both (B) and (D), data are presented as mean ± SD; n ≥ 50 cells; and the groups were compared using a non-parametric Student's t test. *p < 0.05, **p < 0.01, ****p < 0.0001.

(E) Western blot analysis (with PAF1/PD2 and RAD52 antibody) of chromatin fractions and corresponding whole cell lysate (WCL) from indicated cells after treatment with cisplatin or

gemcitabine. Histone H2B and β-actin were used as a loading control for chromatin fraction and WCL, respectively.

(F) Western blot analysis represents the level of YH2AX in indicated cells following PAF1/PD2 knockdown and chemotherapeutic treatment.

(G) Confocal analysis shows the co-localization of PAF1/PD2 and YH2AX in HeLa cells after treatment with cisplatin for 48 h. Scale bars, 2 μm.

(H) Scr and siPAF1/PD2 U2OS cells were subjected to NHEJ, HR, and SSA assays, and quantification was performed using flow cytometry. The data are presented as the mean ± SD; n = 3. **p < 0.01. In all immunoblot images, relative densitometric values are provided below the blot images after normalizing to H2B (for chromatin fraction) and β-actin (for WCL).

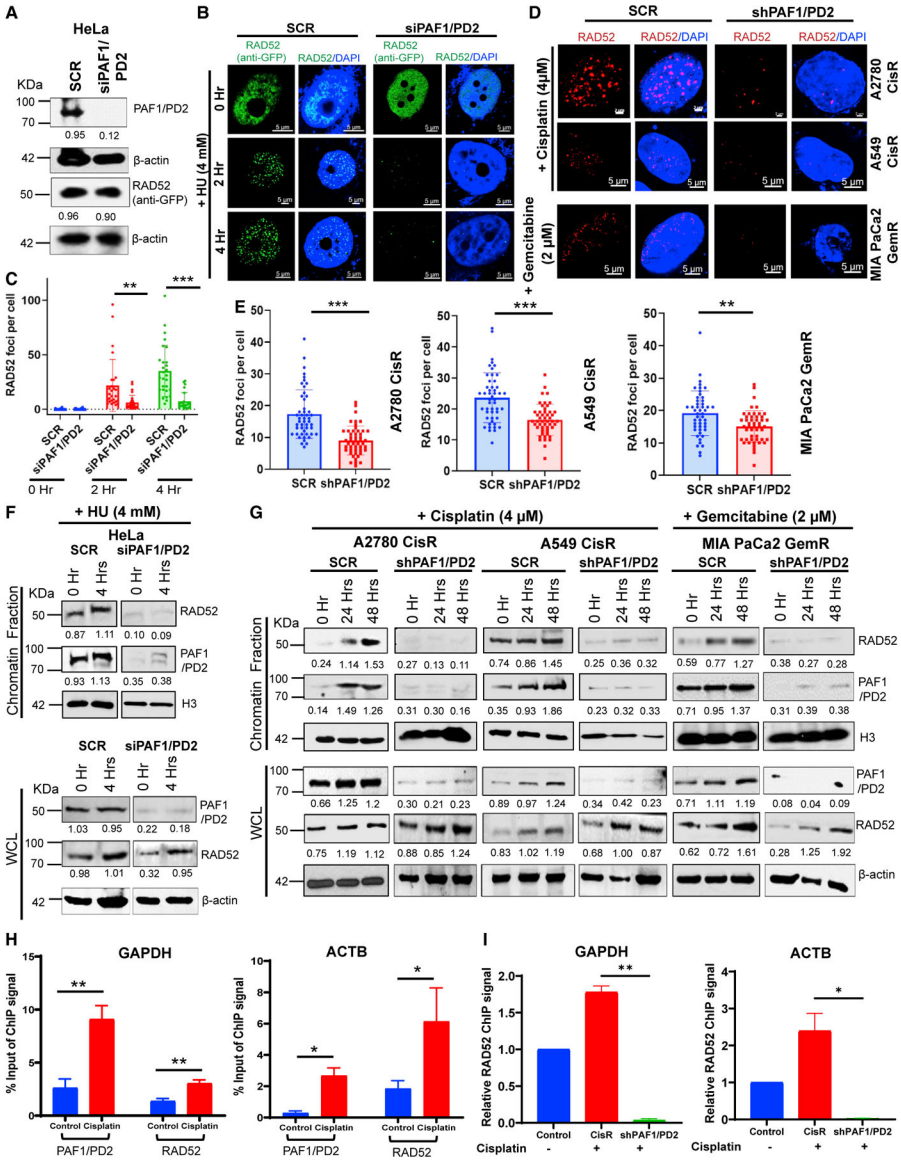

Figure 5. RAD52 recruitment to chromatin is reduced in PAF1/PD2-deficient cells

(A) Immunoblot analysis on GFP-RAD52-expressing HeLa cells shows the knockdown of PAF1/PD2. β-Actin was used as a loading control.

(B) Representative confocal microscopy showing GFP-RAD52-repair foci in PAF1/PD2-silenced HeLa cells on treatment with HU for indicated time points. Scale bars, 5 μm.

(C) Graph represents the number of RAD52 foci per cell in the indicated groups. Data are presented as mean ± SD; n ≥ 30 cells. Scale bars, 5 μm..

(D and E) Scr and PAF1/PD2 knockdown cells were immunostained with anti-RAD52 antibody. Representative immunofluorescence images are shown in (D), and RAD52 foci numbers in cells were counted and presented as a graph in (E). Scale bars, 5 μm. Data are presented as mean ± SD; n ≥ 50 cells.

(F and G) Western blot analysis of chromatin fraction and WCL demonstrate reduced binding of RAD52 to chromatin on PAF1/PD2 knockdown and treatment with HU (F) or

cisplatin/gemcitabine (G) in the indicated cells. H3 and β-actin were used as a loading control for chromatin fraction and WCL, respectively. In all immunoblot images, relative densitometric values are provided below the blot images after normalizing to H3 (for chromatin fraction) and β-actin (for WCL).

(H) ChIP assay illustrates the recruitment of PAF1/PD2 and RAD52 in transcriptionally active GAPDH and ACTB gene on treatment with cisplatin.

(I) The effect of PAF1/PD2 knockdown on the recruitment of RAD52 to the GAPDH and ACTB gene using ChIP assay with RAD52 antibody in A2780 cells after treatment with cisplatin (4 μM). Data are presented as mean ± SD; n = 3.

The effect of PAF1/PD2 knockdown in bar charts was compared with the respective controls (transfected with Scr) by nonparametric Student's t test. *$p < 0.05$, **$p < 0.01$, ***$p < 0.001$.

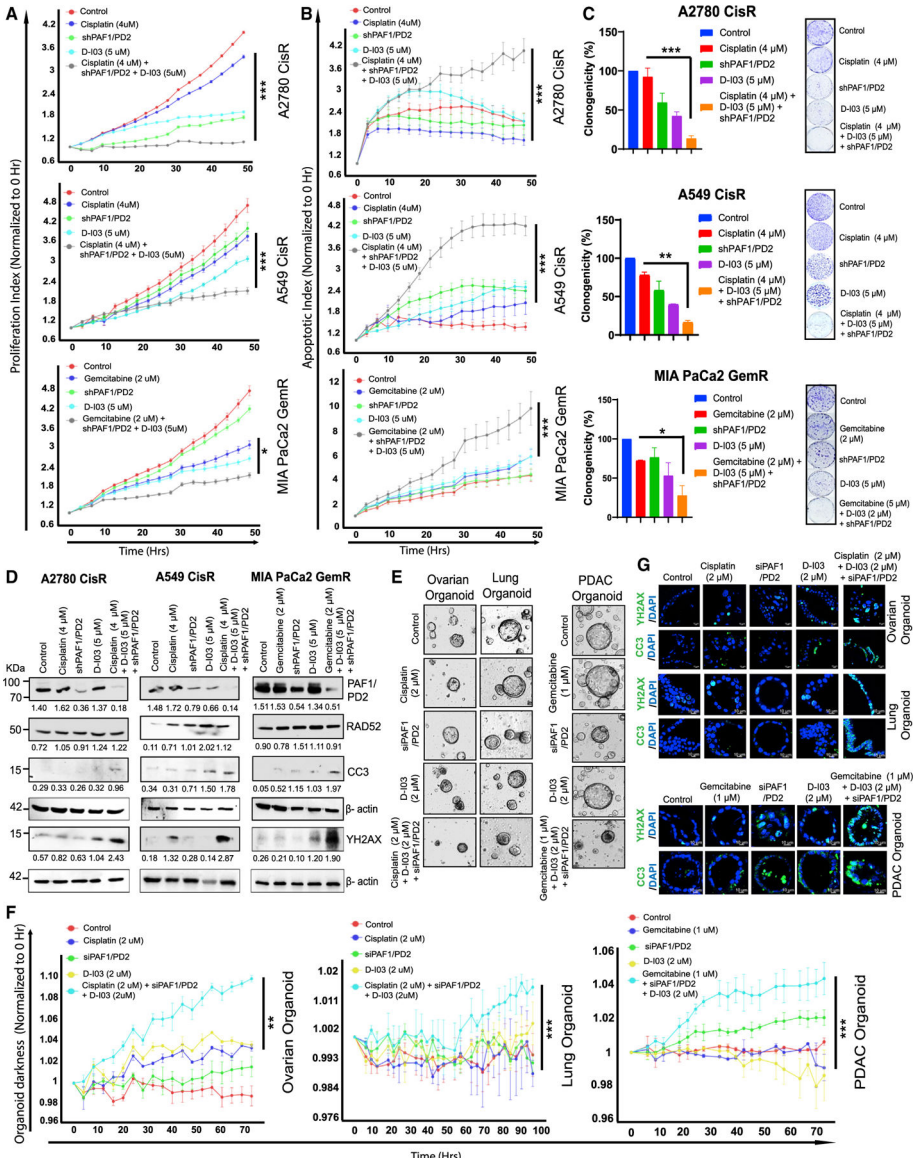

Figure 6. Pharmacological inhibition of RAD52 and PAF1/PD2 silencing improves chemotherapy sensitivity

(A and B) Proliferation (A) and apoptotic (B) index demonstrate the effect of RAD52 inhibitor (D-I03; 5 μM), along with PAF1/PD2 knockdown and cisplatin (4 μM) or gemcitabine (2 μM) treatment in chemoresistant cells, respectively, for 48 h as determined by Incucyte live-cell imaging system. For both graphs in (A) and (B), 3,000 cells/well were seeded as described in the star methods, and five 10× images per well were taken every 3 h. Data are presented as mean ± SEM; n = 3.

(C) Colony formation assay demonstrates the effect of cisplatin or gemcitabine, D-I03, and PAF1/PD2 knockdown alone or the combination of all three on the growth of chemotherapeutic resistance cells. Data are presented as mean ± SD; n = 3.

(D) Representative western blots in indicated cells are presented. Relative densitometric values are provided below the blot images after normalizing to β-actin.

(E and F) Representative (E) and quantitative (F) real-time kinetics of organoid darkness in indicated organoids. Images are representative of respective experimental endpoints taken using the Incucyte system. Data are presented as mean ± SEM; n = 3. For E, Scale bar, 1,000 μm.

(G) Confocal images of YH2AX and CC3 staining in a representative organoid treated as indicated. Scale bars, 10 μm.

Effects of combination treatment were compared with the respective cisplatin or gemcitabine treatment alone by nonparametric Student's t test. *$p < 0.05$, **$p < 0.01$, ***$p < 0.001$.

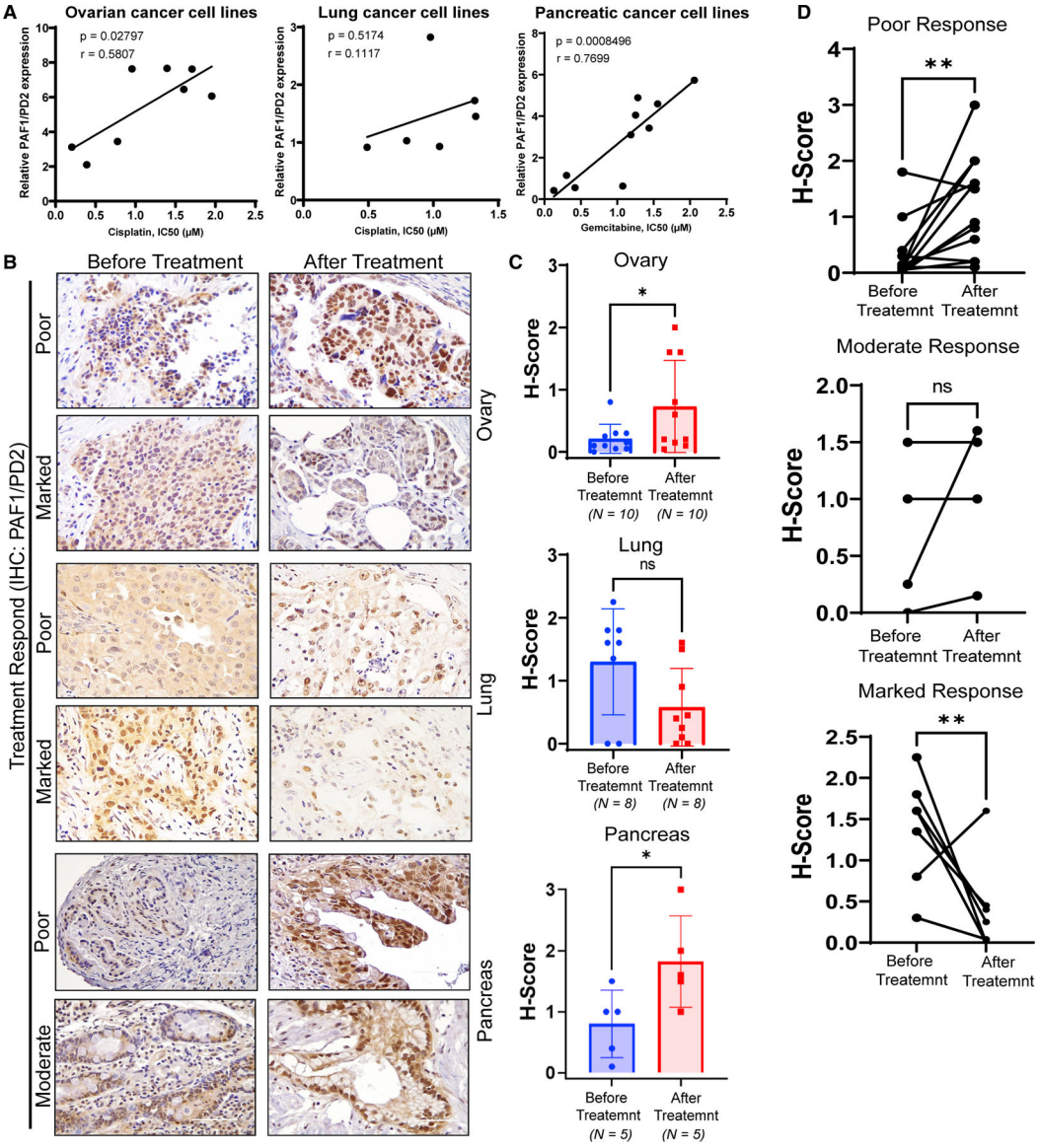

Figure 7. PAF1/PD2 predicts chemotherapy vulnerability in human ovarian, lung, and pancreatic cancers

(A) Correlation between PAF1/PD2 expression and cisplatin IC_{50} or gemcitabine IC_{50} in cancer cell lines as shown in Figure S8.

(B and C) Representative (B) and quantitation (C) of PAF1/PD2 expression through IHC analysis compared between before and after chemotherapy in ovarian (n = 10), lung (n = 8), and pancreatic (n = 5) cancer patients. For B, Scale bars,200 μm.

(D) Statistical analysis combining all three cancer types illustrates the correlation of PAF1/PD2 expression after chemotherapy in patients with poor, moderate, and marked response to chemotherapy.

For all graphs, data are presented as mean ± SD. *p < 0.05, **p < 0.01, ***p < 0.001. See also Table S3.

KEY RESOURCES TABLE

REAGENT or RESOURCE	SOURCE	IDENTIFIER
Antibodies		
Anti-PAF1/PD2 antibody	Bethyl Laboratories	Cat# IHC-00378; RRID: AB_1547992
Anti-RAD52 antibody	Abcam	Cat# ab117097; RRID: AB_10901779
Anti-Ki67 antibody	Cell Signaling	Cat# 12202S; RRID: AB_2620142
Anti-Cleaved caspase 3	Cell Signaling	Cat# 9661L; RRID: AB_2341188
Anti-YH2AX	Cell Signaling	Cat# 9718S; RRID: AB_2118009
Anti-PAF1/PD2	This Paper	N/A
Anti-PAF1/PD2 antibody	Abcam	Cat# ab20662; RRID: AB_2159769
Anti-RAD52 antibody	Santacruz	Cat# sc-365341; RRID: AB_10851346
Anti-GFP antibody	Novus Biologicals	Cat# NB600-308; RRID: AB_10003058
Anti-RAD51 antibody	Abcam	Cat# ab133534; RRID: AB_2722613
Anti-RPA32 (total) antibody	Abcam	Cat# ab109084; RRID: AB_10861764
Anti-RPA32 (phospho)	Bethyl laboratories	Cat# A300-245A; RRID: AB_210547
Anti-CtIP antibody	Santacruz	Cat# sc-271339; RRID: AB_10608728
Anti-PAF1/PD2 antibody	Bethyl Laboratories	Cat# A300-172A; RRID: AB_309394
Anti-Histone H2B antibody	Santacruz	Cat# sc-515808
Anti-β-actin antibody	Millipore Sigma	Cat# A5441; RRID: AB_476744
Universal HRP-conjugated Secondary antibody	Vector Laboratories	Cat# MP-7500; RRID: AB_2336534
HRP-conjugated rabbit secondary antibody	Invitrogen	Cat# 32460; RRID: AB_1185567
HRP-conjugated rabbit secondary antibody	Invitrogen	Cat# 32460; RRID: AB_1185567
Chemicals, Peptides, and Recombinant Proteins		
Cisplatin	Millipore Sigma	Cat# C2210000
Gemcitabine	Millipore Sigma	Cat# G6423-10MG
Lipofectamine 2000	ThermoFisher	Cat# 11668027
DMSO	Sigma	Cat# D2650
Matrigel	Corning	Cat# 356234, 356,255
Dynabeads	Invitrogen	Cat# 10–003-D
LightCycler 480 SYBER Green I Master mix	Roche	Cat# 04707516001
Collagenase II	Millipore Sigma	Cat# C7657
Propidium Iodide	ThermoFisher	Cat# P1304MP
RNase A	ThermoFisher	Cat# EN0531
Dispase	ThermoFisher	Cat# 17105041
IncuCyte Annexin V Orange dye	Sartorius	Cat# 4759
IncuCyte Annexin V Green dye	Sartorius	Cat# 4624
IncuCyte cytotox green reagent	Sartorius	Cat# 4633
Critical commercial assays		
OxiSelect Comet Assay kit	Cell Biolabs	Cat# STA-351

REAGENT or RESOURCE	SOURCE	IDENTIFIER
Duolink PLA multicolor kit	Sigma	Cat# DUO96010
iScript cDNA Synthesis Kit	Bio-Rad	Cat# 1708891
ChIP DNA clean & concentrator kit	Zymo Research	Cat# D5205
Deposited data		
Mass Spectrometry data	This paper, Pride ProteomeXchange	10.6019/PXD039281
Experimental models: Cell lines		
A549	ATCC	Cat# CCI-185
H292	ATCC	Cat# CRL-1848
H358	ATCC	Cat# CRL-5807
H2122	ATCC	Cat# CRL-5985
H23	ATCC	Cat# CRL-5800
SW1573	ATCC	Cat# CRL-2170
SKOV3	ATCC	Cat# HTB-77
OVCAR3	ATCC	Cat# HTB-161
CAOV-3	ATCC	Cat# HTB-75
PA1	ATCC	Cat# CRL-1572
SW626	ATCC	Cat# HTB-78
MIA PaCa2	ATCC	Cat# CRL-1420
SW1990	ATCC	Cat# CRL-2172
AsPC-1	ATCC	Cat# CRL-1682
BxPC-3	ATCC	Cat# CRL-1687
CD18/HPAF	ATCC	Cat# CRL-1997
Capan-1	ATCC	Cat# HTB-79
A2780	Millipore Sigma	Cat# 93112519
COV362.4	Millipore Sigma	Cat# 07071904
S2VP10	Dr. Ashok K Saluja	N/A
SUIT-2	Dr. Michel Ouellette	N/A
T3M4	Dr. S.G. Gordon	N/A
COLO357	Dr. Oshawa	N/A
U2OS-DR	Dr. Jeremy Stark	N/A
U2OS-EJ5	Dr. Jeremy Stark	N/A
U2OS-SA	Dr. Jeremy Stark	N/A
Experimental models: Organisms/strains		
Athymic Nude Mouse	Envigo	N/A
Human ovarian cancer tissue microarray	US Biomax	Cat# OV721
Human lung cancer tissue microarray	US Biomax	Cat# LC10013c
Human pancreatic cancer tissue microarray	US Biomax	Cat# T141c
Paraffin-embedded deidentified human tissue samples	UNMC tissue bank	N/A
Oligonucleotides		

REAGENT or RESOURCE	SOURCE	IDENTIFIER
Primers for qPCR	Invitrogen	(See Table S4)
Primers for ChIP	Invitrogen	(See Table S4)
Recombinant DNA		
siRNA targeting PAF1/PD2 and corresponding non-targeting controls (Scr)	Origene	Cat# SR310177
PAF1 plasmid	Origene	Cat# RC200103L3
Software and alogorithms		
ImajeJ	ImajeJ	https://imagej.net/software/imagej/
GraphPad Prism 8.02	Graphpad	https://www.graphpad.com/